

AD-A044 568

STANFORD UNIV CALIF DEPT OF PHYSICS
FUNDAMENTAL EXPERIMENTS AT LIQUID HELIUM TEMPERATURES.(U)
AUG 77 W M FAIRBANK, J M MADEY

F/G 20/13

F44620-75-C-0022

UNCLASSIFIED

AFOSR-TR-77-1207

NL

AD
A044568



END
DATE
FILMED

10-77

DDC

AD A044568

AFOSR-TR- 77- 1207

Physics Department
Stanford University
Stanford, California

ANNUAL REPORT

to the

OFFICE OF AEROSPACE RESEARCH

AIR FORCE OFFICE OF SCIENTIFIC RESEARCH

for

FUNDAMENTAL EXPERIMENTS AT LIQUID HELIUM TEMPERATURES

Present Air Force Contract No. F44620-75-C-0022

For Period 1 October 1975 to 30 September 1976

PRINCIPAL INVESTIGATORS: William M. Fairbank
Professor of Physics

John M. J. Madey
Senior Research Associate

Approved for public release;
distribution unlimited.



AIR FORCE OFFICE OF SCIENTIFIC RESEARCH (AFSC)
NOTICE OF TRANSMITTAL TO DDC
This technical report has been reviewed and is
approved for public release LAW AFR 199-12 (7b).
Distribution is unlimited.
A. D. BLOSE
Technical Information Officer

| REPORT DOCUMENTATION PAGE | | READ INSTRUCTIONS BEFORE COMPLETING FORM |
|--|-----------------------|--|
| 1. REPORT NUMBER AFOSR TR- 77- 1207 | 2. GOVT ACCESSION NO. | 3. RECIPIENT'S CATALOG NUMBER |
| 4. TITLE (and Subtitle) FUNDAMENTAL EXPERIMENTS AT LIQUID HELIUM TEMPERATURES | | 5. TYPE OF REPORT & PERIOD COVERED Interim |
| 7. AUTHOR(s) William M. Fairbank John M. J. Madey | | 6. PERFORMING ORG. REPORT NUMBER |
| 9. PERFORMING ORGANIZATION NAME AND ADDRESS Department of Physics Stanford University Stanford CA 94025 | | 8. CONTRACT OR GRANT NUMBER(s) F44620-75-C-0022 |
| 11. CONTROLLING OFFICE NAME AND ADDRESS AFOSR/NP Bolling AFB, Bldg. 410 Wash DC 20332 | | 10. PROGRAM ELEMENT, PROJECT, TASK AREA & WORK UNIT NUMBERS 61102F 2301/A5 |
| 14. MONITORING AGENCY NAME & ADDRESS (if different from Controlling Office) Annual 4 repl. 1 Oct 75 - 30 Sep 76 | | 12. REPORT DATE 11 August 1977 |
| | | 13. NUMBER OF PAGES 67 |
| 16. DISTRIBUTION STATEMENT (of this Report) Approved for public release; distribution unlimited. | | 15. SECURITY CLASS. (of this report) Unclassified |
| 17. DISTRIBUTION STATEMENT (of the abstract entered in Block 20, if different from Report) | | 15a. DECLASSIFICATION/DOWNGRADING SCHEDULE |
| 18. SUPPLEMENTARY NOTES | | |
| 19. KEY WORDS (Continue on reverse side if necessary and identify by block number) | | |
| 20. ABSTRACT (Continue on reverse side if necessary and identify by block number) During the past contract year important new results have been obtained in the surface shielding experiment and in the polarized He(3) experiment. In this period the temperature transition in the anomalous surface shielding effect was discovered and investigated. A complete report/thesis was written covering all the shielding effect work to date. In the polarized He(3) experiment measurements were made of the longitudinal nuclear relaxation times of dilute mixtures of polarized He(3) in liquid He(4) (molar concentrations of 7×10^{-3}) at 4.2 K in magnetic fields between 36×10^{-6} G and 2 mG in order to search | | |

332578

DDC
SEP 26 1977
INFORMATION

for techniques which would allow the achievement of very long relaxation times. By using a solid H(2) wall coating in a 1-cm diameter cell, a relaxation time in excess of five days was obtained. Fabrication of all internal components of the prototype electron/positron thermalizer was completed during the past contract year. The central apparatus was assembled and wired. A laboratory was equipped, necessary cryogenic and vacuum equipment was constructed, and preparations were made for low temperature runs of the thermalizer prototype during the 1976-77 contract year.

2000 100 000000 000 00000000
00000000 00000000

| | |
|----------------------------------|---|
| ACCESSION for | |
| NTIS | White Section <input checked="" type="checkbox"/> |
| DDC | Buff Section <input type="checkbox"/> |
| UNCLASSIFIED | |
| 15 11 1977 | |
| DISSEMINATION/AVAILABILITY CODES | |
| S. CHAL | |
| A | |

UNCLASSIFIED

TABLE OF CONTENTS

| | PAGE |
|--|------|
| I. INTRODUCTION | 1 |
| II. RESEARCH RESULTS | 2 |
| A. Investigation of Anomalous Surface Shielding Using the Slow Electron Time-of-Flight Technique | 2 |
| 1. Background | 2 |
| 2. Progress During the Report Period | 5 |
| B. Electron/Positron Thermalizer and Photon Counting Detector | 12 |
| 1. Background | 12 |
| a) Photon Counting Millimeter Wave Detector . . . | 13 |
| b) Positron Source | 20 |
| 2. Progress During the Report Period | 23 |
| C. Nuclear Spin Lattice Relaxation of Dilute Mixtures of Polarized He^3 in Liquid He^4 in Low Magnetic Fields . . | 25 |
| 1. Background | 25 |
| 2. Progress During the Report Period | 25 |
| a) Experimental Technique | 25 |
| b) Experimental Results and Analysis | 28 |
| c) Conclusions | 39 |
| III. REFERENCES | 41 |

APPENDICES

- A1. Evidence for a Temperature-Dependent Surface Shielding Effect in Cu
- A2. Apparatus for Measuring the Force of Gravity on Freely Falling Electrons
- A3. Experimental Evidence for a Temperature-Dependent Surface Shielding Effect Inside a Copper Tube
- B. Photon Counter Performance Estimates

I. INTRODUCTION

During the past contract year important new results have been obtained in the surface shielding experiment and in the polarized He^3 experiment. In this period the temperature transition in the anomalous surface shielding effect was discovered and investigated.¹ A complete report/thesis was written covering all the shielding effect work to date. In the polarized He^3 experiment measurements were made of the longitudinal nuclear relaxation times of dilute mixtures of polarized He^3 in liquid He^4 (molar concentrations of 7×10^{-3}) at 4.2 K in magnetic fields between 36 μG and 2 mG in order to search for techniques which would allow the achievement of very long relaxation times. By using a solid H_2 wall coating in a 1-cm diameter cell, a relaxation time in excess of five days was obtained.

Fabrication of all internal components of the prototype electron/positron thermalizer was completed during the past contract year. The central apparatus was assembled and wired. A laboratory was equipped, necessary cryogenic and vacuum equipment was constructed, and preparations were made for low temperature runs of the thermalizer prototype during the 1976-77 contract year.

II. RESEARCH RESULTS

A. Investigation of Anomalous Surface Shielding Using the Slow Electron Time-of-Flight Technique

1. Background

Our work with the anomalous electrostatic shielding effect grew out of a series of experiments which were performed in order to search for a temperature dependence in the ambient axial electrostatic potential variations inside a vertical copper tube. A vertical metal tube subject to the gravitational field of the Earth is expected to have spatial variations in electrostatic potential along its axis because of several mechanisms which cause the walls of such a tube to depart from the normal uniform charge distribution found in a single metallic crystal not in a gravitational field. One mechanism results from the fact that a macroscopic metal tube is composed of very many small crystals which, because of their differing work functions, develop contact potential differences from one crystal to the next in order to achieve a single electrochemical potential throughout the entire metal. The presence of the Earth's gravitational field produces two effects. First, the center of mass of the conduction electrons in the walls of the tube is shifted downward a small but finite amount (approximately 10^{-31} m), resulting in a downward electric field in the metal of mg/e. This field must exist in the metal if the conduction electrons are to be in equilibrium in the presence of a downward gravitational field of magnitude g. The existence of this field was first predicted by Schiff and Barnhill in 1966.² Second, gravity causes a differential compression of the ionic lattice of the walls. The metallic electrons redistribute in an effort to maintain charge neutrality throughout the metal; however, the cancellation of the large field resulting from the positive charge density gradient is not complete because of the finite compressibility of the electron gas (we are using a very simple model of the

metal; however, the conclusions are correct). The result is an upward electric field in the metal of magnitude roughly Mg/e where M is the ion mass. The existence of a field of approximately the same value outside the surface of the metal was first predicted in 1967 by Dessler, Michel, Rorschach, and Trammel.³

Interest in the nature of the ambient electrostatic potential variations along the axis of a copper tube was stimulated by the 1967 experiment of Witteborn and Fairbank⁴ (described in Appendix A2) which measured the force of gravity on a single electron by means of a time-of-flight technique. Two aspects of the results of that experiment did not agree with the theoretical predictions concerning the ambient potential variations to be found along the axis of the copper tube employed as an electrostatic shield in the time-of-flight measurements. First, it proved possible to control the distribution of electron flight times by the use of applied fields in the copper tube as small as 2.5×10^{-11} V/m. In particular, it was possible to turn back the slowest electrons in the beam by applying these very small fields. Such a result is not compatible with the expected patch effect potential fluctuations, which on the most straightforward model can have RMS values as large as 10^{-6} V or so. We have shown that any electrons which could pass through a region having potential fluctuations of this size would have their flight times modified only infinitesimally by a field of 2.5×10^{-11} V/m applied over a 1-m flight path. Specifically, the applied field would not be able to turn back such electrons. Second, the electron gravity measurement indicated that the only forces larger than 5×10^{-12} eV/m acting on an electron traveling along the axis of the copper tube were gravity and a force due to the field predicted by Schiff and Barnhill. The 10^{-7} eV/m force predicted on the basis of the ion lattice distortion was not observed.

Considerable controversy arose concerning the proper reconciliation of the results of the Witteborn-Fairbank experiment with the theoretical predictions about the ambient potential fluctuations inside the shielding tube. Other workers conducted a variety of experiments to search for the existence of a lattice distortion field both inside and just outside a metal subject to a compression gradient. These experiments verified the order of magnitude predictions of the theory. It must be pointed out however that these experiments were conducted under conditions quite different from those of the Witteborn-Fairbank experiment. One of the more obvious differences is the temperature: Witteborn and Fairbank worked at 4.2°K in order to make use of superconducting magnets and circuitry while all other experiments to date which look at the lattice distortion field outside a metal have been done at room temperature. Witteborn and Fairbank,^{4,5} among others,^{6,7} suggested that a surface shielding effect occurring at low temperatures might shielded the interior of the copper tube from fields arising in the walls of the tube. Assuming that the charge responsible for the surface shielding is provided by electrons in a layer which is decoupled from both the strain gradient and the electron distribution present in the tube walls, the patch effect and lattice distortion fields would not appear along the tube axis, while the Schiff-Barnhill field produced by the surface electrons would be present. This situation would agree completely with the results of the Witteborn-Fairbank experiment.

If a surface shielding effect of the type described exists at 4.2°K, it presumably does not exist at room temperature since there was no evidence of its presence in the room temperature experiments which studied the lattice distortion field; it would thus be a temperature-dependent shielding effect. We felt that by conducting electron time-of-flight

experiments at temperatures from 4.2° K to room temperature we could determine whether or not such a temperature-dependent shielding effect exists and if so, the range of temperatures over which it is operative.

The initial phase of our search for a temperature-dependent surface shielding effect consisted of using a modified version of the Witteborn-Fairbank apparatus in an attempt to determine the room temperature ambient potential fluctuations in the copper tube. This work was followed by a similar measurement at LN₂ temperature. These measurements indicated that any onset of anomalous surface shielding would occur below LN₂ temperature. After conducting a 4.2° K run to verify the existence of the shielding effect at that temperature we made a quick check on the ambient field present at a temperature of about 20° K; these runs indicated that the transition to the anomalous surface shielding condition must occur between 4.2° K and 20° K. In order to search for the transition, we then designed a low-power drift tube heating and temperature monitor system which would make possible experiments in which the drift tube operated at temperatures from 4.2° K up to 30-40° K while the other components of the apparatus remained at 4.2° K. This mode of operation has the great advantage of permitting the use of superconducting magnets and circuitry as well as cryopumping. The ability to use these techniques results in a factor of 10⁴ improvement in sensitivity over the version of the apparatus employed at 300° K and 77° K thus allowing a sensitivity in the temperature range from 4.2° K to 30° K equal to the sensitivity achieved at 4.2° K in the original electron free fall work.

2. Progress During the Report Period

From October 1975 through January 1976 the drift tube heating and temperature monitor system was installed and a low temperature run

was conducted. The sensitivity achieved in this run allowed a rather clearcut determination of the ambient electric field present in the tube at several temperatures from 4.2° K to 11° K. The data from this run were analyzed and a Ph.D. thesis/report was written from February through July of 1976.

The results of the heated drift tube work are summarized in Fig. A1 along with the earlier results at 300° K and 77° K and are shown in an expanded view in Fig. A2. Note particularly in the figures that the ambient force appears to increase by several orders of magnitude when the temperature is increased from 4.2° K to 4.5° K. These results, coupled with the results of the original electron free fall experiment and the room temperature results of various experiments, indicate that there is a surface shielding effect at 4.2° K; the effect is greatly weakened when the temperature of the tube is increased by only 0.2° K and is either non-existent or else extremely small above 6° K. The ambient electric field observed in the tube above 6° K is in good agreement with the predictions of Dessler, Michel, Rorschach, and Trammel for the magnitude of the lattice distortion field. It seems that the patch effect fluctuations are somewhat smaller than expected on the basis of commonly accepted models, although patch effect fluctuations may contribute to the total ambient field seen in the drift tube above 6° K. The details of this work are described in the Ph.D. thesis of James M. Lockhart, which is enclosed as a part of this progress report. The work also led to a publication in Physical Review Letters during the present contract year; copies of that paper are also enclosed (Appendix A1).

The heated drift tube experiments have proven to be extremely

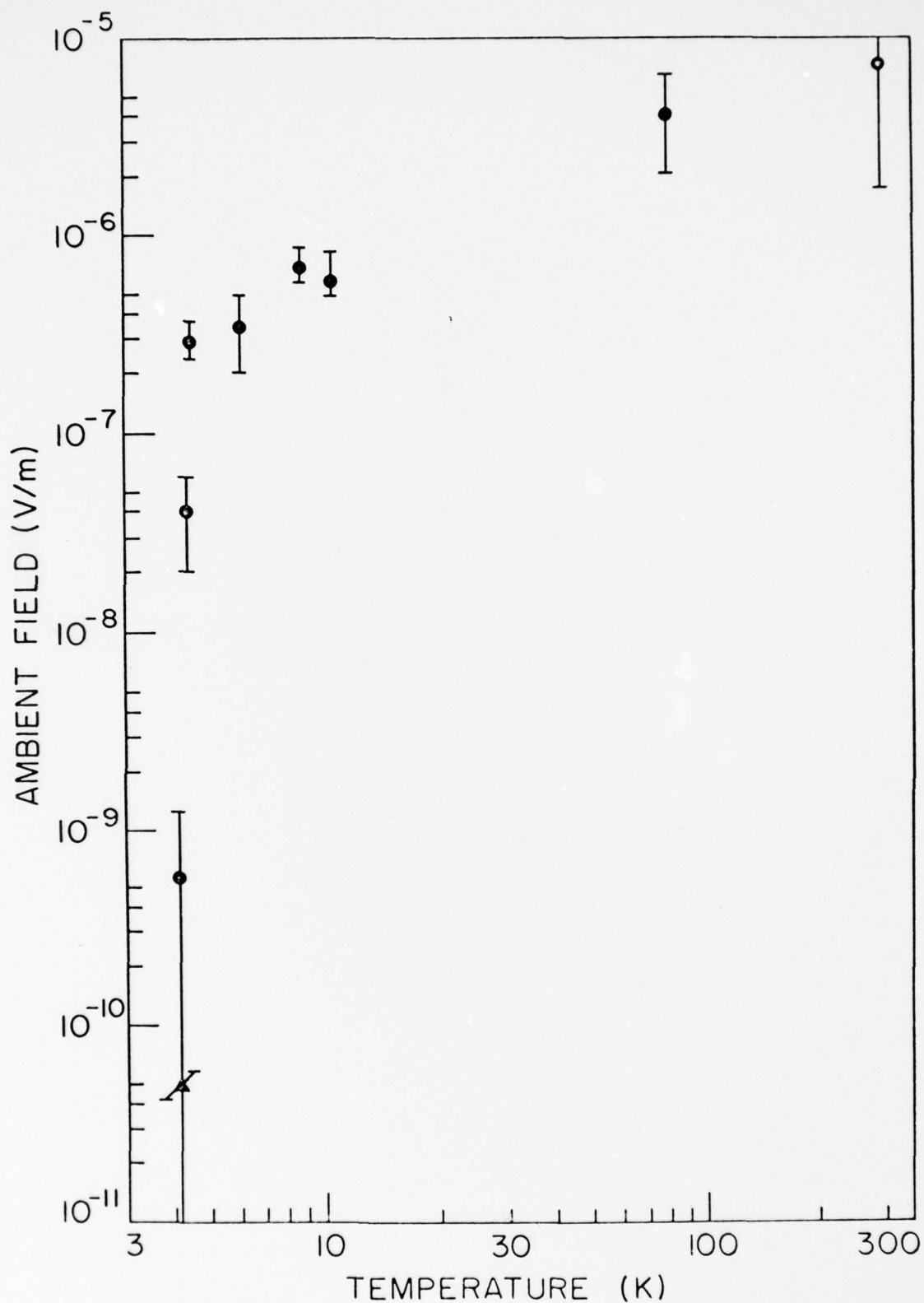


Figure A1. The ambient electric field in the tube as a function of tube temperature. The closed circles show the present experimental results. The triangle shows the absolute value of the 1967 result of Witteborn and Fairbank, which was -5×10^{-11} V/m at 4.2 K.

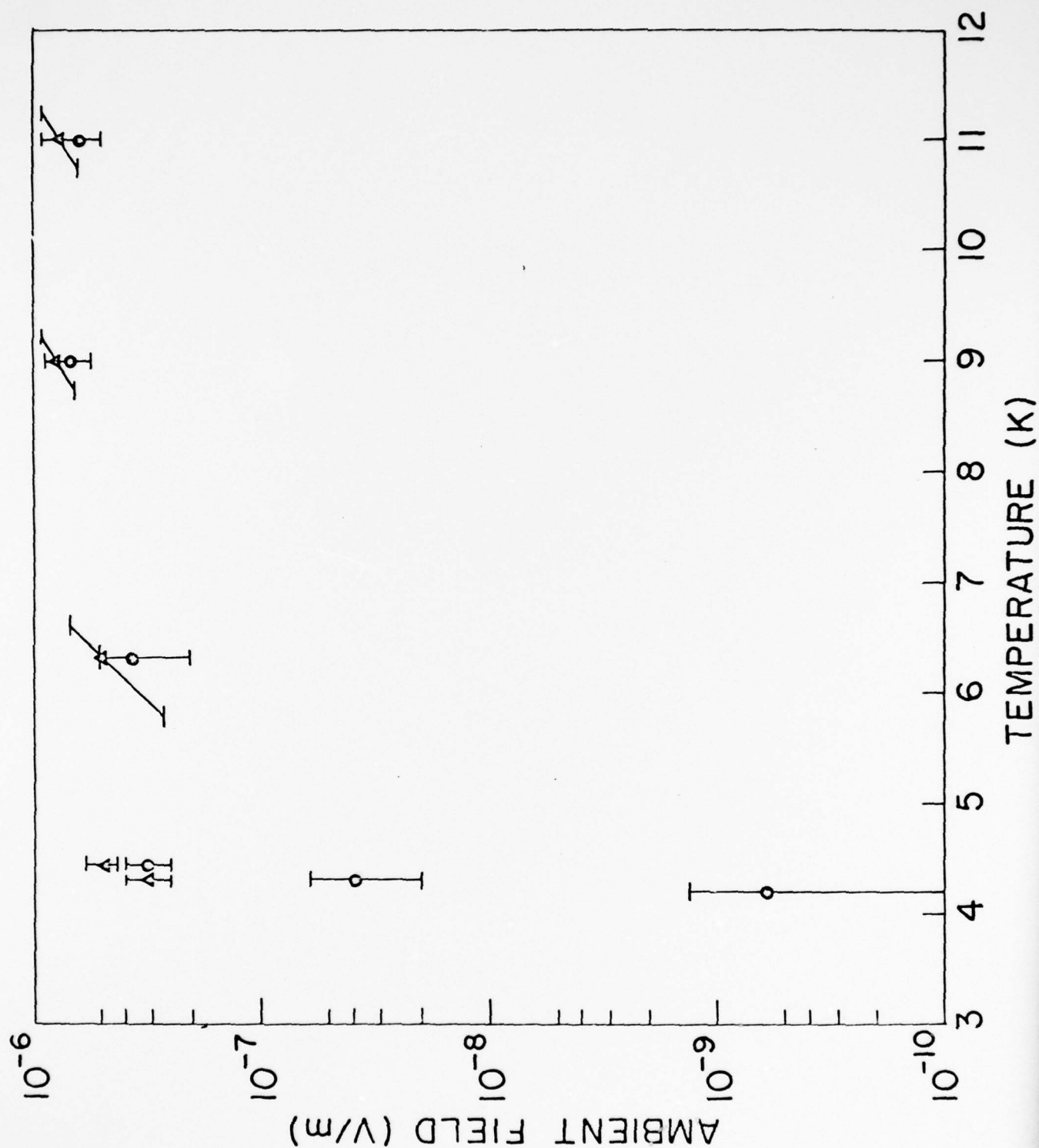


Figure A2. An expanded view of the low-temperature results. The two sets of points are obtained using different analysis techniques, as described in the text.

important to the study of the shielding effect since they established the temperature region in which the shielding effect disappears. However, the strongest evidence for the existence of the effect at 4.2° K is provided by the very accurate determination of the ambient electric field in the tube obtained in the electron free-fall experiment. We present in Figure A3 a summary of the results of that experiment, which shows that the net force on an electron traveling through the tube is equal to the applied force for applied force values ranging over three orders of magnitude. The solid line is a least square fit to the experimental data; it indicates that the net potential gradient in the tube with no applied force is $0 \pm 5 \times 10^{-12}$ eV/m. It seems that the only reasonable interpretation of this result is that the only ambient fields present in the tube are the gravitational field and the Schiff-Barnhill field arising from a surface electron layer; the surface electrons act to shield the interior of the tube from lattice distortion and patch effect fields arising in the walls of the tube. Because of the renewed interest in this earlier work generated by the new results, some effort during August and September of 1976 was devoted to the writing of a comprehensive review of the original electron free fall apparatus. This work continued into the present contract year and resulted in a publication in Review of Scientific Instruments (enclosed as Appendix A2).

Toward the end of the 1975-1976 contract year we also began an evaluation of theoretical models for the shielding mechanism. The bulk of this work was performed during the 1976-77 contract year and will be described in the next interim report.

In August and September of 1976 we also began designing apparatus modifications for a new low temperature run in which shielding

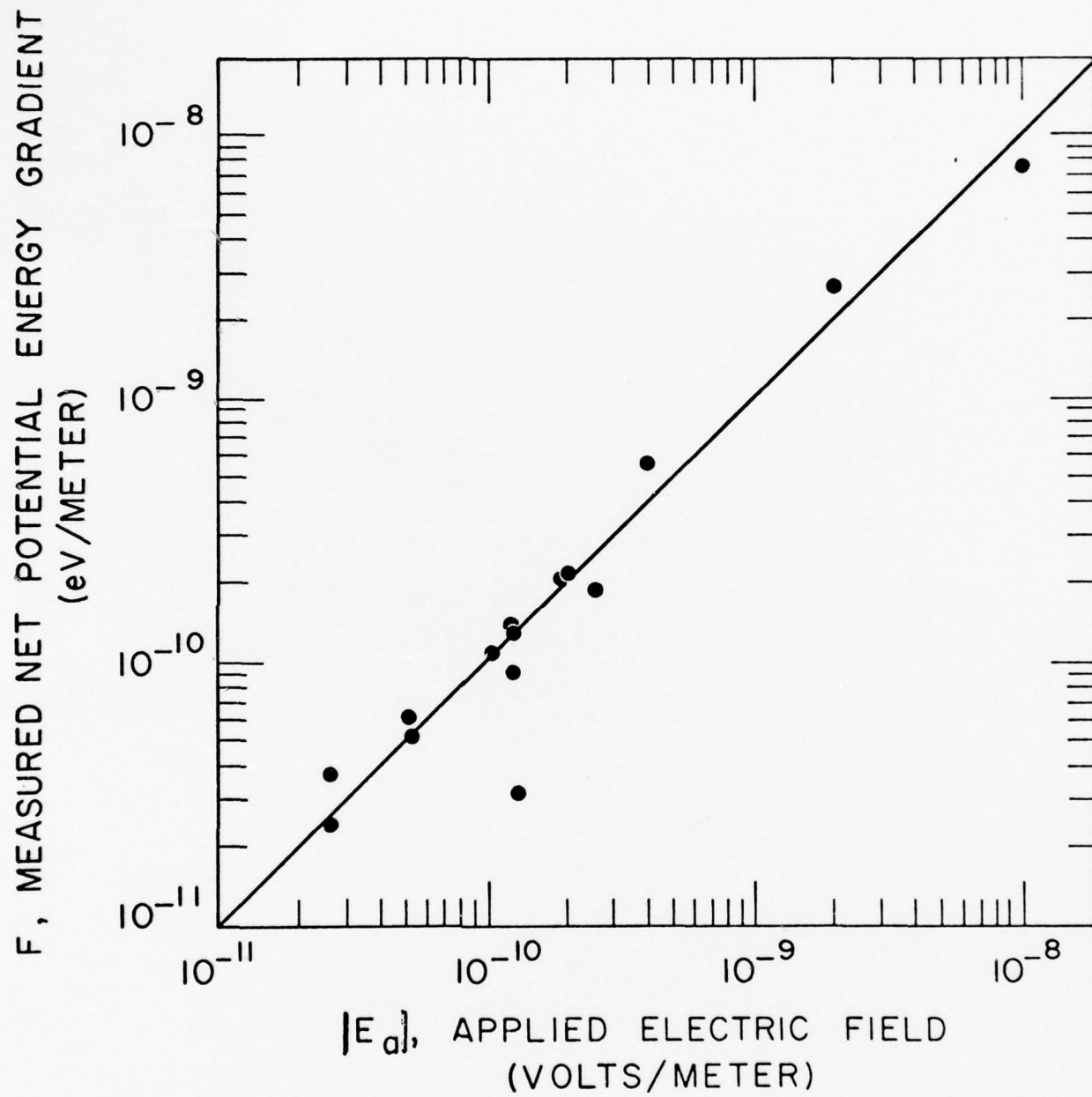


Figure A3

effect measurements would be taken at temperatures both lower and more closely spaced than in the previous work. Such runs are now in progress.

B. Electron/Positron Thermalizer and Photon Counting Detector

1. Background

We have designed a thermalizer system which accepts a beam of electrons or positrons having an energy spread of 1 eV or so and uses eddy current losses and resonant energy exchange to thermalize the beam to 4°K. Adiabatic expansion to 10^{-2} - 10^{-3} °K is then employed to reduce the beam energy to 10^{-7} eV. When used with electrons, this system can be configured to serve either as an improved electron source for the time-of-flight studies or as a photon counting detector operating in the millimeter wave region. When used with low energy positrons obtained from the channeled polyethylene absorber system previously developed in this laboratory,⁸ the thermalizer can provide a source of 10^{-7} eV positrons for the time-of-flight experiments. Thermalization is carried out with the particles in a very high vacuum so that annihilation losses are negligible.

Since the two different configurations of the thermalizer employ the same principles of operation, knowledge gained from tests of either version is immediately applicable to the other version. Since the photon counter configuration is the simpler of the two, our strategy has been to assemble that version of the apparatus and conduct tests with it in order to optimize various device parameters. Based on the knowledge gained in the current testing program, we will proceed to assemble the second version of the thermalizer, incorporating any modifications these tests may indicate.

We describe below first the operation of the photon counter and second the operation of the positron source. A positron source can be converted to an electron source by changing the input stage and reversing the bias potentials.

a) Photon Counting Millimeter Wave Detector

Description of Operation: Operation of the detector is based on the interaction of the incident radiation with a distribution of low energy electrons trapped in a solenoidal magnetic field. The electrons are in the magnetic ground state and the maximum kinetic energy is maintained below $\hbar\omega$. If the radiation is in the neighborhood of the cyclotron frequency it can excite the $n=0 \rightarrow n=1$ transition and the excited electron will escape the trap and be counted.

A schematic of the source is shown in Figure 1. As a first approximation, the electrons are constrained to move along the magnetic field lines. Control of the electron distribution is accomplished by potentials applied to the cylindrical electrodes surrounding the electron distribution.

All elements of the detector except the energy analyzer, part of the transfer gate and the surface barrier detector as located inside the main solenoid whose field determines the frequency of operation. A field of 25 kOe is required at 4 mm and 100 KOe at 1.0 mm. Interaction of the radiation and the electrons occurs inside a high Q TE_{011} mode cavity. The cavity is tunable through mechanical motion of the end plates.

The energy analyzer and surface barrier detector are located in a field one tenth the strength of the main field. The potential of the energy analyzer is set just high enough to reflect the $n=0$ electrons in the trapped distribution. The $n=1$ electrons which have absorbed a photon from the radiation field acquire a kinetic energy equal to $0.9 \hbar\omega$ in the transition from the strong to the weak field. These electrons

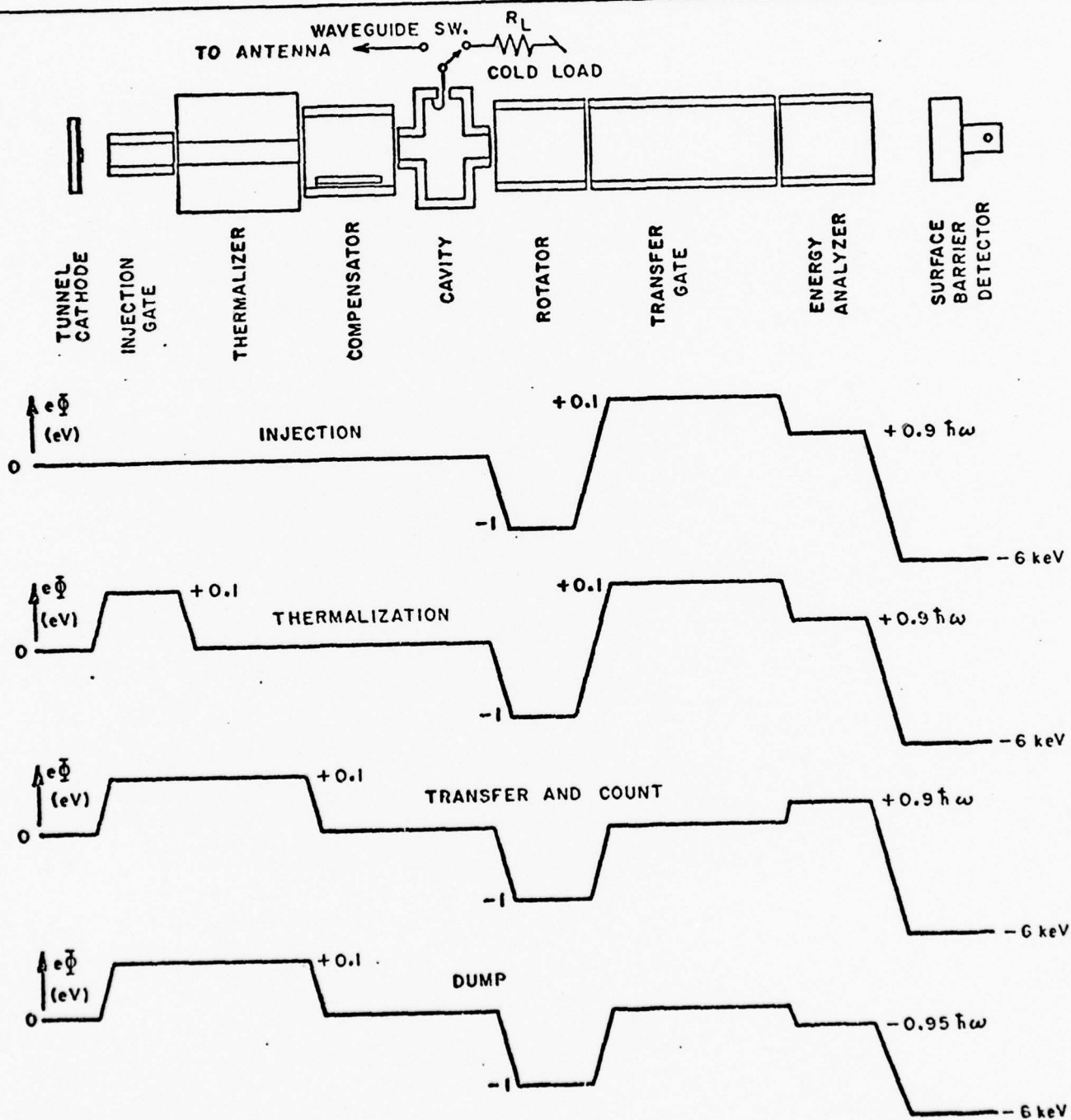
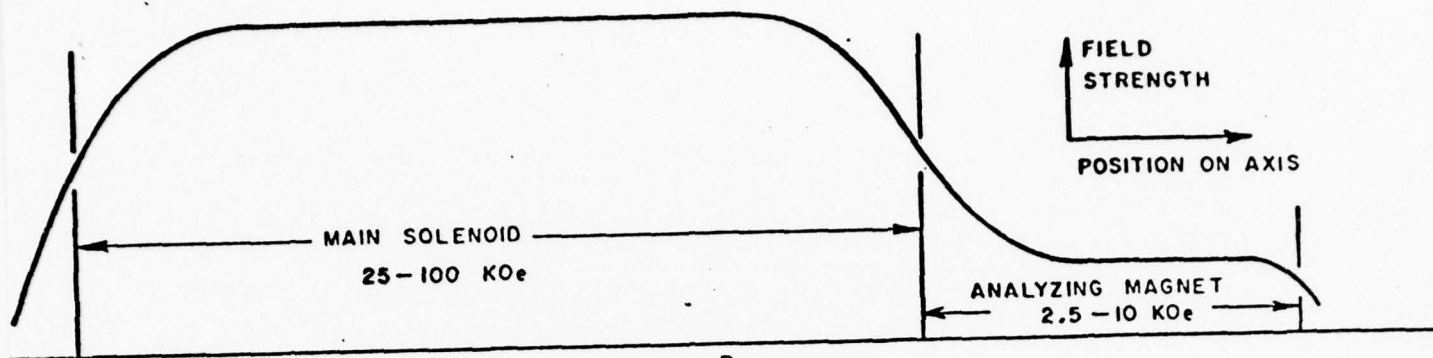


FIGURE 1

pass through the energy analyzer, are accelerated to 6 keV and counted in the surface barrier detector.

Operation of this detector can be described as occurring in five sequential stages. The first three stages (injection, thermalization, and transfer) serve to generate a reservoir of low energy electrons. Electrons are exposed to the incident radiation and counted in stages 4 and 5 (count and dump).

In the injection stage the input gate is lowered so as to permit entry of a low current electron beam from a thin film tunnel cathode. A current of 10 μA from the cathode will result in a linear density of electrons in the trap of approximately 10^6 cm^{-1} . The injection gate is then closed trapping these electrons in the section comprised of the thermalizer, compensator, cavity and rotator.

The walls of the thermalizer are made of a conductive ceramic. In the thermalization cycle the trapped electrons transfer their kinetic energy to the charge carriers in the wall of the tube. Their cyclotron energy is transferred by radiation in the cavity to the load resistor R_L . The load resistor is coupled to the microwave cavity on one arm of a spdt waveguide switch. Calculations indicate that electrons will lose energy exponentially during the thermalization cycle with a time constant less than 10 milliseconds. The time required to reach thermal equilibrium at 4 K is estimated to be less than 80 milliseconds.

In the transfer stage the potential of the ceramic thermalizer is adiabatically raised while the potential of the transfer gate is adiabatically lowered while the waveguide switch transfers the cavity from the load resistor to the feedline. At the conclusion of

the transfer stage the trapped electrons can no longer exchange energy with the bath via the thermalizer and the load resistor. The principal mechanism by which the trapped electrons gain energy after transfer is through irradiation in the microwave cavity. Noise on the biasing potentials can also transfer energy to the distribution but this effect can be reduced to negligible proportions.

The fraction of the trapped electrons in the magnetic ground state with kinetic energy less than $\hbar\omega$ depends on the temperature and the magnetic field, e.g., the operating frequency. At 4° and 4 mm only 25% of the trapped electrons will have the appropriate energy. (The number grows to 90% at 1 mm.) All the rest will have sufficient energy to pass through the energy analyzer on their first path through the transfer gate. Only electrons with the appropriate energy will remain in the trap at the completion of the transfer cycle.

Electrons emerging from the trap during transfer are not counted. During the detection cycle the counting electronics are activated and the emerging electrons are counted for a predetermined interval of time. At the end of the detection cycle the potential on the energy analyzer is lowered to dump all the remaining trapped electrons (the dump cycle). The ratio of the number of electrons ejected during the detection cycle to the total number of electrons in the trap is a measure of the probability for a cyclotron transition. Knowledge of the cavity Q, the time spent in the cavity and the transition probability, permits a determination of the energy density of the radiation in the cavity, e.g., of the power level of the incoming radiation.

The sensitivity of the detector can be adjusted by controlling the potential on the cavity relative to the rest of the trap. This

affects both the mean number of electrons in the cavity and the time spent in the trap.

Electron Stability: Trapping lifetimes--from injection to dump--of the order of a second are required for operation of the detector. Attainment of such lifetimes is not a trivial matter since there are several physical processes which can move the electrons in the trapped distribution across the magnetic field lines and into the walls of the trap.

These processes can arise from transverse electric fields due to variations in the work function at the surface or to uncompensated charge accumulations on dust motes or insulating inclusions, diffusion due to scattering from the residual gas, and from deformations of the magnetic field lines.

The associated drift or diffusion rates vary as $1/B$ or $1/B^2$ and so become less of a problem as the field is increased. Diffusion due to scattering, in particular, ceases to be a problem at field strengths above 25 KOe and gas pressures below 10^{-8} torr. But even at 100 KOe the drift due to transverse electric fields is a serious problem. A potential difference of 50 μ V across the walls of the trap will drive the electron distribution to the walls in less than a second for a 2 mm trap i.d.

A technique is available for stabilization of the electron distribution against transverse electric fields and B field curvature. The technique relies on the observation that the drift velocity, considered as a vector field, is fixed in position relative to the walls of the trap and the guide solenoid.

If the drift velocity assumes a single value when averaged over the length of the trap the drift will average to zero if the electron distribution is rotated about the trap axis at a rate rapid in comparison to the time required to drift across the trap.

The means of accomplishing this rotation can be built into the geometry of the electric field between the electrodes surrounding the electrons. This field will always have a radial component off axis which will interact with the axial magnetic field to induce a net rotation of the electron distribution. The electrodes must be designed to insure that even the slowest electrons in the distribution are rotated rapidly enough to guarantee stability. Rotation is accomplished in the photon counter during passage of the trapped electrons between the cavity and the "rotator" in Figure 1.

If the averaged drift velocity has a gradient, the rotation of the distribution can result either in exponential radial expansion or contraction of the distribution depending on the direction of the gradient. Stability, e.g., exponential contraction, can be assured by deliberate introduction of a gradient with the appropriate direction which is large enough to dominate any pre-existing gradient.

A pair of strips parallel to the axis embedded in but insulated from the wall of one of the cylindrical electrodes provide an appropriate means of introducing the required gradient. One of the strips is biased positive, the other negative relative to the wall. The strips are included in the "compensator" shown in Figure 1.

Performance Estimates: Table 1 lists the calculated quantum efficiency noise temperature, and response time of the photon counter at several wavelengths between 1 and 4 mm for the specified values of

TABLE 1

| Wavelength | Unloaded Cavity Q (Q_c) | Electronic Q (Q_E) | Quantum Efficiency | Radiometric Noise Temperature | Response Time |
|------------|-----------------------------------|---------------------------|-----------------------|----------------------------------|---------------|
| 3.8 mm | 10^4 | 3×10^5 | 3.3 % | 2.3 K | 20 nsec |
| 3.3 mm | 9.1×10^3 | 4×10^5 | 2.2 % | 2.2 K | 16 nsec |
| 2.0 mm | 4.1×10^3 | 2×10^6 | 0.11% | 1.4 K | 4 nsec |
| 1.0 mm | 2.2×10^3 | 1.3×10^7 | 0.02% | 0.4 K | 1.2 nsec |

cavity and electronic quality factors. The physical analysis upon which this table is based appears in appendix B.

b) Positron Source

Description of Operation: Analysis of typical TOF distributions in the electron free fall experiment indicates that ground state electrons of energy less than 10^{-7} eV were accumulated at the rate of one every 10-100 seconds. A somewhat higher rate would be desirable from the standpoint of counting statistics while a lower rate would require unacceptably long running times. With respect to the positron source, the general limits on intensity of one ground state positron every 1-100 seconds with an energy less than 10^{-7} eV provide useful guidelines with respect to the required source performance.

The intensity of natural β emitters fails to approach this goal by many orders of magnitude. The rate of emission of ground state positrons in a 10 KOe magnetic field is at most of the order of $10^{-6} \text{ sec}^{-1} \text{ eV}^{-1}$ for a one curie Co^{58} source. The probability of emission into a 10^{-7} eV range is therefore less than $10^{-13} \text{ sec}^{-1}$. Focusing techniques alone cannot improve the situation since the phase space density is a conserved quantity in a non-dissipative system.

The approach being pursued is to capture a small number of positrons in a stable trap and to rely on dissipative mechanisms and adiabatic expansion to reduce their temperature to the millikelvin range. A high vacuum can be maintained in the trap so that the annihilation rate during storage is negligible. The trapped positrons can be thermalized directly to 4° or below depending on the ambient temperature. Provided that the trap is emptied adiabatically,⁹ the temperature of the distribution can be reduced to the order of 10 millikelvin, i.e., to less than 10^{-6} eV.

Thermalization to 4° proceeds through three distinct processes. Prior to capture in the trap, positrons from an isotope source pass through thin polyethylene absorber. Those positrons which come to rest within a thousand angstroms of the exit side of the absorber have a good probability of diffusing out of the absorber. Experimentally, the positrons emitted from the absorber are found to have an energy spread of several eV.

Thermalization to 4° is carried out in the vacuum. The positrons are constrained (neglecting ExB drifts, etc.) to move along the field lines in a solenoidal magnetic field. Positive electrostatic potentials at the ends of the trap constrain the axial motion of the particles.

The trapped positrons, kinetic and cyclotron energy must be separately thermalized. The mechanism for the reduction of the kinetic energy is eddy current damping while the mechanism for the cyclotron states relies on the enhancement of the radiative transition rate.

The positrons in the trap pass alternately along the axis of the tube with thick resistive walls and a microwave cavity resonant at the cyclotron frequency. The image charge on the walls of the tube take a finite time to rearrange itself. The image charge therefore fails to shield the charge carriers in the walls if the positrons are in motion. Penetration of the E field into the walls results in joule heating of the tube and a concomitant loss in energy by the positrons.

The calculated rate of loss of energy is a function of the radius of the tube and the resistivity. For positrons of moderate energy the rate of loss of energy is proportional to the positron kinetic

energy. Loss rates of a factor of e in less than 5 milliseconds are possible for 1 eV positrons in a 2 mm diameter tube.

By contrast, the cyclotron motion of the positron does not require significant realignment of the image charge distribution and is not affected by the presence of the tube. However, perturbation theory indicates that the radiative transition rate depends linearly on the density of final states and the density of states can be increased by orders of magnitude by enclosing the positron in a microwave cavity resonant at the cyclotron frequency. The process can be viewed as the resonant exchange of energy between the electromagnetic field in the cavity and the positron's cyclotron motion. With a cavity $Q = 10^4$, resonant exchange results in a rate of cyclotron energy comparable to that obtainable for the kinetic energy using eddy current damping. If the cavity is maintained at 4°K and the cyclotron frequency is $1.5 \times 10^{11} \text{ sec}^{-1}$, the bulk of the trapped positrons will end up in the cyclotron ground state. One half of these will be in the magnetic ground state.

Assuming a thermal distribution and use of adiabatic expansion, the experiment can be performed using one positron per pulse. Successful operation of the source then depends on the efficiency with which particles can be captured from the beam of positrons diffusing out of the absorber. The fundamental problem is that the volume of the trap is necessarily limited while the density of positrons in the beam is small. The probability of capture in flight, as by abruptly lowering and raising the trapping potentials, is too small to be of practical interest.

Practical capture efficiencies are predicted for a process wherein dissipation within the trap leads to capture. In the process

the isotope and absorber are located in a 1 kOe field and the trap in a 50 kOe field. The absorber must be biased at a positive potential to insure that positrons emitted from the absorber with high cyclotron energies can enter the trap. With the appropriate choice of biasing potentials, radiation of just one photon by a positron within the trap can lead to capture. The calculated capture efficiency for the source design is 10^{-3} based on a 5 eV spread in cyclotron and kinetic energy at the absorber.

2. Progress During the Report Period

During the beginning of the contract period effort on the electron/positron thermalizer was focused on completing the fabrication of all components for the main electrode section of the prototype thermalizer. Assembly and wiring of the main apparatus began in May of 1976. This period also saw the renovation of a laboratory to accommodate the thermalizer experiment. Construction of the necessary cryogenic systems (dewar, He gas recovery manifold, pumps, transfer lines, level gauge) was begun in August of 1976 and was completed in October of 1976. Construction of the high vacuum system and the detector circuitry was also begun in August and was brought nearly to completion by October 1976.

Low temperature runs with the prototype thermalizer are now in progress; measurements should include an evaluation of the suitability of the present eddy current thermalization section, determination of maximum trapping time, measurement of the Q of the microwave cavity, and finally the flux of electrons having energies $\leq 10^{-7}$ eV. Since the existing prototype has been assembled in a photon counting detector configuration, we also expect to complete a set of experiments in which blackbody photons from a thermal source are detected in the PCD. These measurements

should indicate the sensitivity and noise temperature of the PCD and its potential as a viable radiation detector for use in such fields as radio astronomy. The results of this work will be described in the next interim report.

C. Nuclear Spin-Lattice Relaxation of Dilute Mixtures of Polarized He^3 in Liquid He^4 in Low Magnetic Fields

1. Background

In order to make a sensitive measurement of the electric dipole moment of the He^3 nucleus¹ or to make a useful He^3 free precession nuclear gyroscope, it is necessary to obtain very long He^3 nuclear relaxation times in a virtually zero magnetic field. In the experiment proposed by Hamilton and Fairbank,² sufficiently long relaxation times were to be obtained by using a sufficiently dilute solution of He^3 in liquid He^4 . It is well known that the intrinsic nuclear relaxation time of a monatomic liquid or gas (i.e., the relaxation due to the interaction between the nuclear spins in the bulk of the sample) is inversely proportional to the density of the nuclear spin.³

It is also well known, however, that other nuclear relaxation mechanisms exist. In particular, the existence of wall-induced nuclear relaxation has been frequently noted in liquid He^3 although the exact nature of the mechanism or mechanisms involved is poorly understood.⁴ In addition, nuclear relaxation due to magnetic field gradients (which is well understood) is prominent in low density He^3 gas⁵ and can be important in low magnetic fields in the liquid as well. Thus, the question of how long the He^3 nuclear relaxation time in low magnetic fields can be made in actual practice by increased dilution with liquid He^4 must be answered experimentally. Our concern here is to report on the results of experiments we have performed in order to answer this question.

2. Progress During the Report Period

a) Experimental Technique

Because of the very small applied fields used in our

experiments ($H_0 \leq 2$ mG typically), the equilibrium thermal polarization is zero for all practical purposes. Thus, in order to measure the spin-lattice relaxation time (T_1) of a sample of He^3 atoms, they must be polarized to an extent which renders the resulting magnetization readily detectable. Fortunately, this is easily accomplished by using an optical pumping process developed by Colegrove, Shearer, and Walters.⁶

In our experiment 300 cm^3 of He^3 gas at 1 torr pressure were typically polarized to $\sim 5\%$ by optical pumping at room temperature. After polarization, He^4 gas which had been previously purified in liquid form by passage through a Vycor superleak, was admitted into the optical pumping bulb. The resulting mixture was then condensed into a Pyrex sample bulb located in the cryostat insert via a 0.5 mm bore Pyrex capillary (see Fig. 1). Our condensed samples typically had a $\text{He}^3 - \text{He}^4$ ratio of 6.9×10^{-4} . The sample bulb was 0.95 cm outside diameter and the final 1 cm of capillary was drawn down to 0.1 mm bore in order to limit diffusion in and out of the sample bulb once it had filled with liquid. It should be noted that during this sample preparation phase, the He^3 is always exposed to a vertical magnetic field which is maintained by Helmholtz coils around the optical pumping bulb, a solenoid around the capillary, and another small set of Helmholtz coils around the sample bulb. The optical pumping field coils and the solenoid are turned off after condensation.

The cryostat insert was immersed in a liquid helium bath at 4.2 K maintained in an 8" i.d. dewar. Thermal contact to the sample was provided by helium exchange gas. The inside of our dewar was lined with a degaussed superconducting Pb foil shield which maintained an ambient field of $\sim 3 \mu\text{G}$ as measured at the sample.⁷ A single μ -metal shield surrounded the outside of the dewar. The presence of the degaussed superconducting

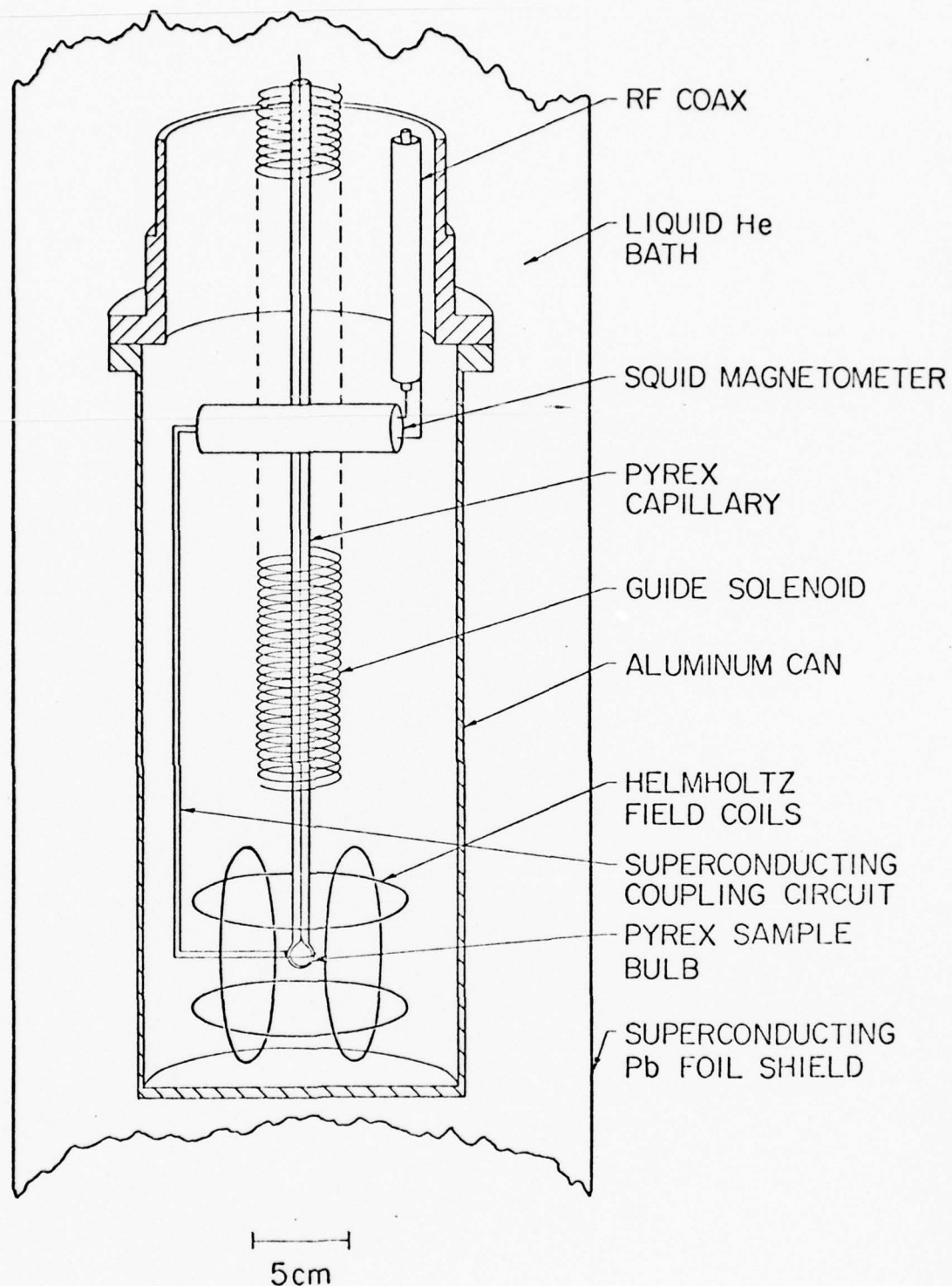


Figure 1. Schematic cross-section of the lower end of the cryostat insert. Helium exchange gas is used to maintain thermal contact with the bath.

shield required that the liquid helium level be kept above the top of the shield at all times and that the cryostat insert be inserted and withdrawn from a cold dewar. The magnetization produced by the polarized He^3 in the sample bulb was detected by an rf-biased SQUID (Superconducting QUantum Interference Device) magnetometer which was coupled to the sample with a persistent superconducting coupling circuit.⁸ Typically, the magnetic field produced by the sample magnetization immediately after condensation was greater than 10 μG yielding a signal to noise ratio in excess of 10^3 in a 1 Hz bandwidth. A signal of this size allowed a number of relaxation measurements to be made before it became necessary to start over again by preparing a new sample.

The actual procedure which was adopted to measure T_1 was an intermittent precession technique. This technique yielded an AC signal which avoided the possibility that magnetometer drift could bias the results. This technique is depicted schematically in Fig. 2. Prior to making a measurement the applied field (H_0 , in the vertical direction) is changed to a standard value, $|\vec{H}_z|$. The measurement of the magnetization is actually made when \vec{H}_x is suddenly switched on ($|\vec{H}_x| = |\vec{H}_z|$). This causes the magnetization \vec{m} to precess in a cone having a half-angle of 45° . The value of $\sqrt{2} |\vec{H}_z|$ was chosen so that the precession frequency was 0.25 Hz. After two complete cycles, \vec{H}_x was switched off, leaving the magnetization again aligned in the z direction. The output of the magnetometer was a 2-cycle sinusoid (with a slight decay in amplitude due to dephasing because of field gradients) whose amplitude was directly proportional to \vec{m} . Figure 3 shows two examples of such measurement.

b) Experimental Results and Analysis

The most striking aspect of our T_1 data is a strong

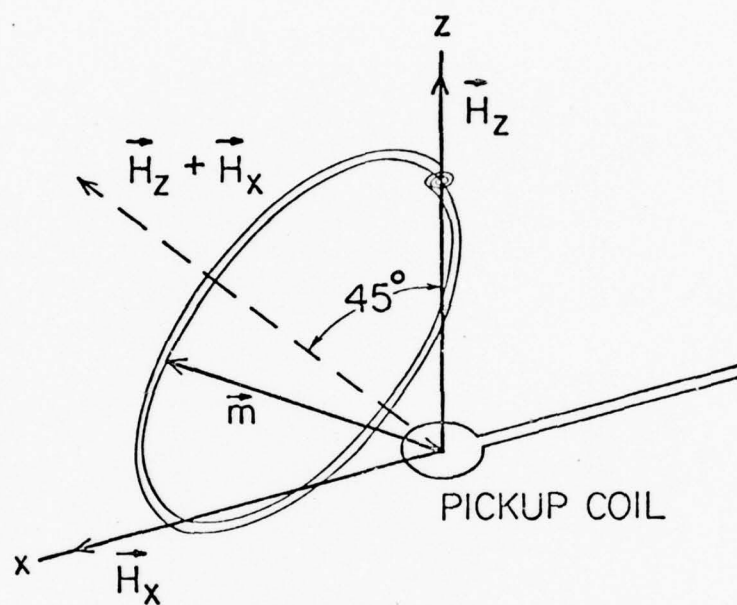


Figure 2. Schematic diagram of the intermittent precession technique used to measure the relative magnitude of the sample magnetization.

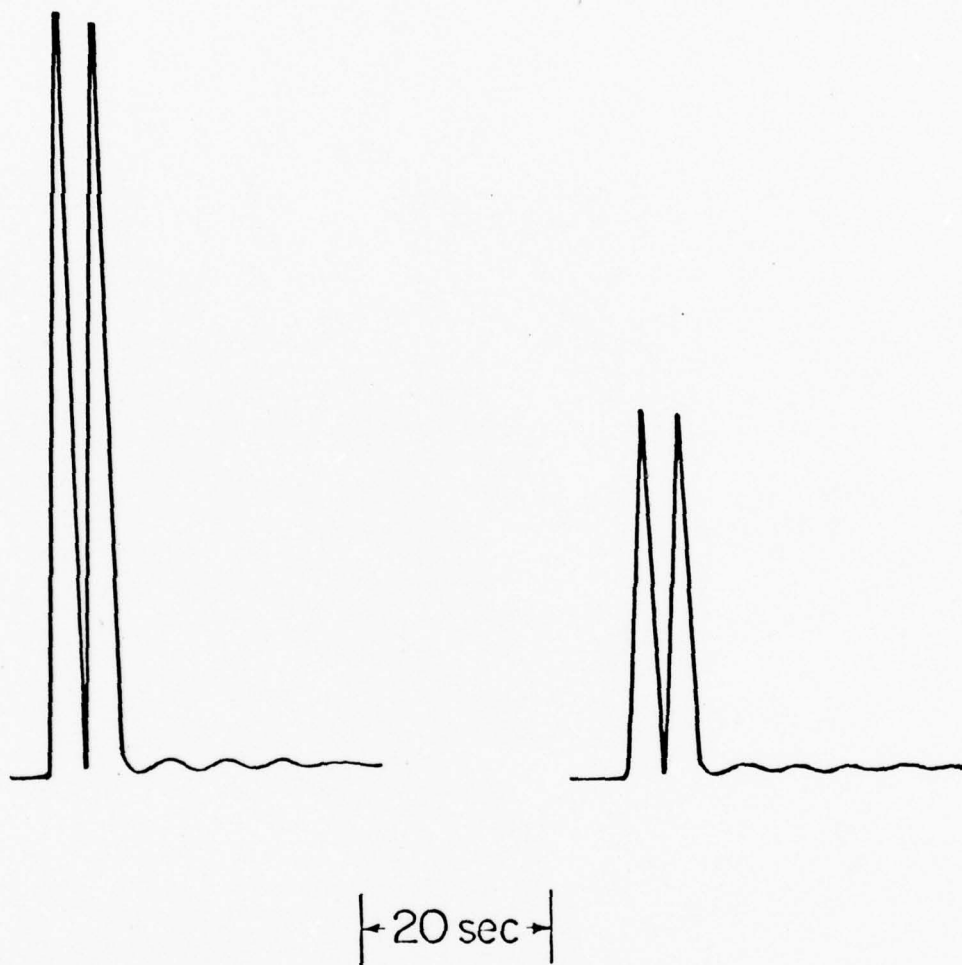


Figure 3. Example of two successive measurements made by the intermittent precession technique. Baseline offset occurring after each measurement is due to dephasing during the precession.

field dependence. For example, in the lowest field we used, $H_0 = 36 \mu\text{G}$, we obtained $T_1 \approx 2.7 \text{ hr}$. As the field is increased, the relaxation time increases and levels off at approximately 2 mG. At this point $T_1 \approx 40 \text{ hr}$. It was experimentally determined that the relaxation rate was independent of the sample location in the shield, small changes in the bath temperature, and whether or not the magnetometer was on. It was ultimately concluded that this field-dependent relaxation was probably due to a ferromagnetic impurity speck located near the sample bulb. In order to discuss this effect, we will first write down the general expression for gradient induced relaxation in a spherical sample (where we will assume that the gradient is uniform) and then discuss the case of a point dipole located near the sample.

The most useful analysis for our purposes of nuclear relaxation due to magnetic field gradients is that done by Barbé, Leduc, and Laloë.⁹ This analysis applies specifically to spherical samples, and since it takes into account the finite size of the sample, it is valid in the limit $\omega_0 \rightarrow 0$ provided the "motional narrowing"³ criterion is met. ($\omega_0 = \gamma H_0$ is the Larmor frequency where γ is the gyromagnetic ratio. For He^3 , $\gamma = 2.038 \times 10^4 \text{ rad. sec}^{-1} \text{ gauss}^{-1}$.) If we specialize their expression to the case of a uniform, axially symmetric gradient, i.e., where the perturbing field H_1 is given by

$$\vec{H}_1 = -\hat{i}Gx - \hat{j}Gy + \hat{k}2Gz$$

and take $H_0 = H_0 \hat{k}$, we obtain

$$(1/T_1)_G = 4(\gamma G)^2 \sum_n \frac{R_0^2}{\beta_{ln}^2 (\beta_{ln}^2 - 2)} \frac{\tau_{ln}}{1 + \omega_0^2 \tau_{ln}^2}$$

where $\tau_{ln} = 1/D(R_0/\beta_{ln})^2$, R_0 is the sample bulb radius, D is the diffusion coefficient and β_{ln} is the n^{th} zero of the derivative of the spherical Bessel function, $j'_l(x)$.

We first consider this expression in the high field limit $\omega_0 \tau_{11} \gg 1$. In our case, this applies for $H_0 \gg 10^{-7}$ gauss; all of our data are in the "high" field limit. In this limit, the expression becomes

$$(1/T_1)_G \approx \frac{4\gamma^2 G^2 D}{\omega_0^2} \sum_n (\beta_{ln}^2 - 2)^{-1} = 2(G/H_0)^2 D, \quad (\omega_0 \tau_{11} \gg 1).$$

Experimentally, we made use of this result by applying a sequence of known gradients to the sample while H_0 was kept constant and then fitting the resulting relaxation rates to the expression $T_1^{-1} = a + bG^2$. We thus obtained a value for the diffusion coefficient of He^3 in liquid He^4 at 4.2 K:

$$D_{34} = 8.4 \pm 0.8 \text{ cm}^2 \text{ sec}^{-1} \quad (\text{see Fig. 4}).$$

It is worth noting that our field-dependent relaxation effect did not fit a H_0^{-2} dependence. Moreover, by using free-precession decays, we were able to estimate the ambient value of G at our sample, and it was determined that it was too small to explain the measured relaxation rates.

Returning to the expression for $(1/T_1)_G$, we now consider the low field limit $\omega_0 \tau_{11} \ll 1$. In this case, the relaxation rate becomes independent of ω_0 and is given by

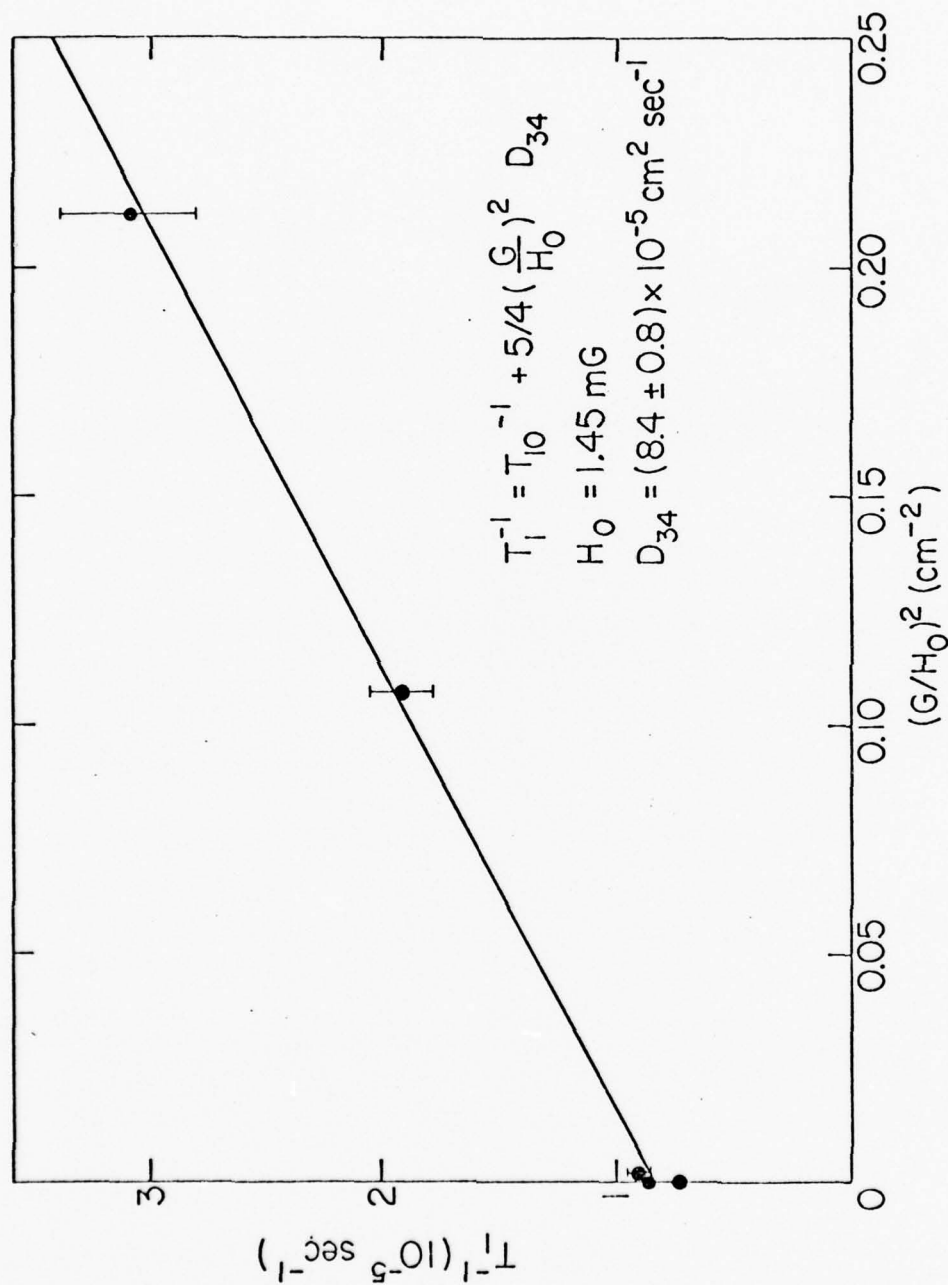


Figure 4. Fit of the relaxation rate data obtained by applying a known uniform gradient. Total applied field was of the form

$$\vec{H} = -\hat{i}Gx + \hat{j}\left(\frac{1}{2}Gy\right) + \hat{k}\left(H_0 + \frac{1}{2}Gz\right).$$

$$\begin{aligned}
(1/T_1)_G &= \frac{4(\gamma G R_0^2)^2}{D} \sum_n [(\beta_{ln}^2 - 2)\beta_{ln}^4]^{-1} \\
&= 0.0914 (\gamma G R_0^2)^2 D^{-1}, \quad (\omega_0 \tau_{11} \ll 1).
\end{aligned}$$

This expression is valid in the "motional narrowing" limit, that is to say, when the relaxation time given by this expression is long compared to $\tau_{11} = 0.231 R_0^2/D$. For our experimental situation, $G \ll 10^{-7}$ gauss cm^{-1} will meet this requirement.

Since, as we have noted, our data do not fit what would be expected if the field-dependent relaxation were due to a uniform gradient, we turn to the possibility of a nearby ferromagnetic contaminant speck. The impact of such a field gradient would be greater on the relaxation rate than it would be on a free-precession decay. We thus consider the situation of a point magnetic dipole, $\vec{\mu}$, located a distance b away from the sample bulb where b is much less than the size of the sample bulb (see Fig. 5). By using an approach similar to the one used to obtain the uniform gradient result together with appropriate simplifications and approximations, we can obtain approximate expressions for relaxation due to an external dipole in the high field ($\omega_0 \tau_d \gg 1$, where $\tau_d = b^2/D$) and the low field ($\omega_0 \tau_d \ll 1$) limits. In the case $\omega_0 \tau_d \gg 1$, we obtain

$$(1/T_1)_d \approx \frac{\pi}{8\sqrt{2}} \frac{\mu^2 \gamma^2 D^{\frac{1}{2}}}{V b^4} \omega_0^{-3/2}$$

where V is the sample volume.

If we plot our data as a function of $H_0^{-3/2}$ (Fig. 6), we see that this model does in fact appear to be appropriate. The value of T_1^{-1} as $H_0^{-3/2} \rightarrow 0$ is then the relaxation rate $(T_1^{-1})_0$ due to remaining

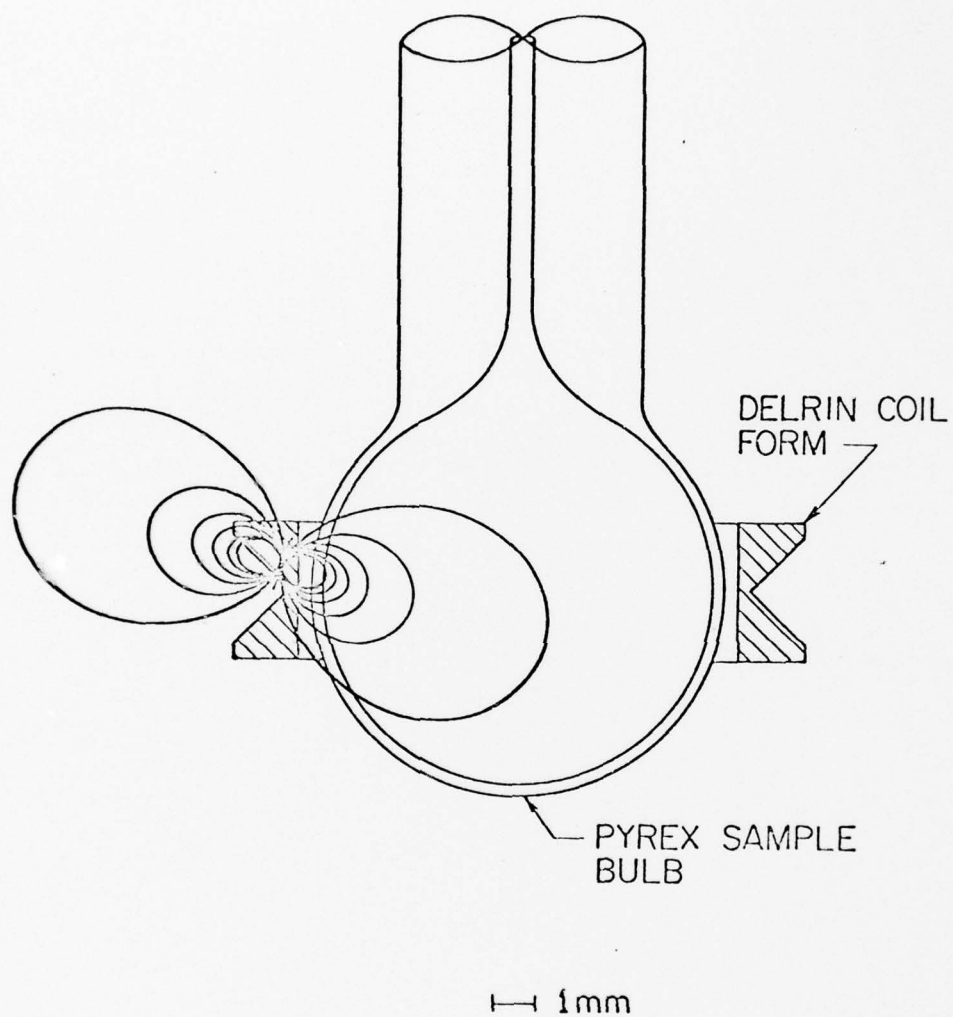


Figure 5. Diagram showing the possible location of a ferromagnetic contaminant dipole. It is assumed that the distance between the contaminant dipole and the sample surface is much less than the sample bulb diameter.

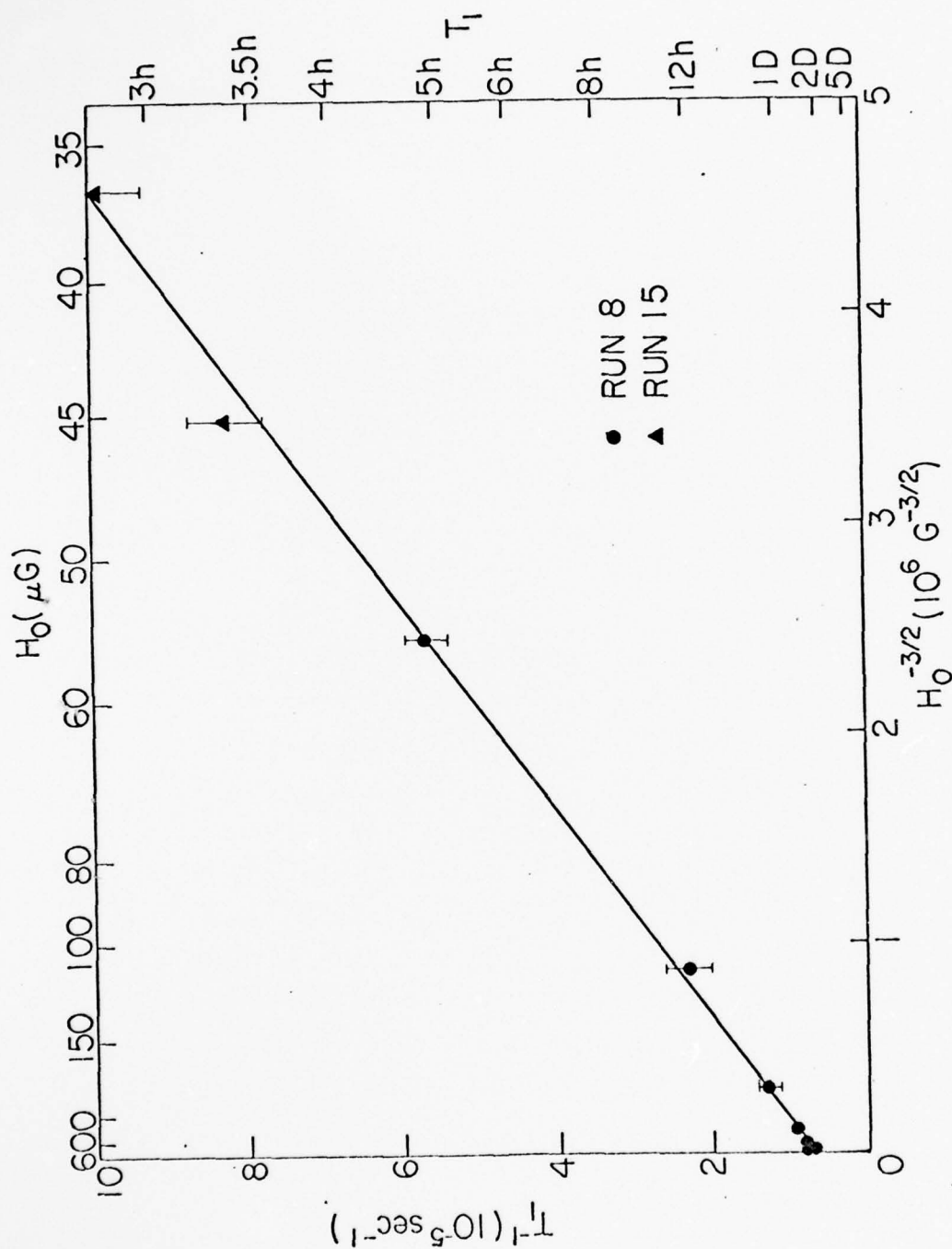


Figure 6. Fit of the relaxation rate data obtained in the bare Pyrex bulb to $H_0^{-3/2}$. The relaxation rate in the limit $H_0^{-3/2} \rightarrow 0$ corresponds to a relaxation time $T_1 \approx 40$ hr.

field-independent relaxation mechanisms such as intrinsic relaxation and relaxation due to wall effects. A least squares fit of our data yields a value $(T_1)_0 = 40.4 \pm 1$ hr and a slope which is appropriate to a dipole $|\vec{\mu}| = 2 \times 10^{-8}$ gauss cm³ located 0.1 cm away, according to the above expression for $(T_1^{-1})_d$.

The Delrin coil form for the magnetometer pickup coil is the only thing this close to the sample. Cabrera,⁷ has measured the remanent magnetization of a number of materials at low fields and low temperature and has found that contaminant dipoles of the size suggested by our data are quite common. In addition, microscopic examination of the coil form has yielded visual evidence of a contaminant speck.

In the case of the low field limit $\omega_0 \tau_d \ll 1$, we again obtain an expression which is independent of H_0 :

$$(1/T_1)_d \approx \frac{\pi}{16} \frac{\gamma^2 \mu^2}{V b D} \quad (\omega_0 \tau_d \ll 1)$$

The motional narrowing condition which must be satisfied in order for this expression to be valid in the limit $H_0 \rightarrow 0$ is

$$\frac{\gamma \mu \tau_d}{b^3} = \frac{\gamma \mu}{b D} \ll 1.$$

If $b = 0.1$ cm, this condition is satisfied when $\mu \ll 4 \times 10^{-10}$ gauss cm³. If this condition is not satisfied, the magnetization of the sample would no longer be uniform,¹⁰ a situation which would be entirely unacceptable for the applications in which we are interested.

The relaxation time of 40 hr seemed to be considerably shorter than what one would expect for intrinsic relaxation. In order to investigate the possibility that relaxation due to wall effects was playing

a significant role, we made use of a discovery made by Barbé, Laloë, and Brossel.¹¹ They found that a number of cryogenic wall coatings (such as H₂, D₂, Ne, Ar, etc.) are effective in suppressing wall relaxation of He³ gas over a limited range of temperatures below the freezing point of the particular wall coating being used. In particular, they found that H₂ was very effective at 4.2 K and obtained a relaxation time of ~ 60 hr instead of the immeasurably short (< 1 sec) relaxation time found in a bare Pyrex bulb.

By loading 1 torr of H₂ into the sample bulb prior to cooling our cryostat, we deposited an estimated 40 molecular layers of hydrogen on the wall of our sample bulb. Relaxation measurements were then made as a function of H₂ and analyzed as described above. In this case we found that $(T_1)_0 = 141 \pm 5$ hr, although the longest time actually measured was 130 hr. This relaxation time in excess of 5 days is longer than any published He³ nuclear relaxation time at low temperatures. (Fitzsimmons, Tankersley, and Walters have reported $T_1 = 250$ hr at 373 K with a 630 torr sample.¹²)

In order to compare our extrapolated relaxation time of 141 hr to a theoretical estimate of the intrinsic relaxation time, we make use of a result obtained by Oppenheim and Bloom for pure liquid He³:¹³

$$T_1^{-1} \approx (1.15) \frac{8\pi\gamma^4 \hbar^2 I(I+1)n_3}{15 Da}$$

where $I = \frac{1}{2}$ for He³, $n_3 = \text{He}^3$ density, a = interatomic distance of closest approach, and D = diffusion coefficient. If we assume that this expression is a reasonable estimate for relaxation of He³ in liquid He⁴ when we take $D = D_{34}$ and the proper value for n_3 , we obtain the estimate $T_1 = 170$ hr. Considering that the values of n_3 and D_{34} are judged to be accurate to

$\pm 10\%$, we see that the extrapolated relaxation time obtained with an H_2 wall coating is close to being limited by the intrinsic relaxation time.

In addition to the H_2 wall coating, we also tried an argon wall coating using the same technique as described for the hydrogen. The reason Ar was chosen is that it is isotopically pure and has no magnetic moment. We found that it had no effect on the relaxation time when compared to the bare bulb result. This is consistent with Barbé, Laloë and Brossel's results; they found Ar to be effective in suppressing wall-induced relaxation only when the temperature was in the 14-36 K range.¹¹

c) Conclusions

The most important conclusion which can be reached on the basis of our experimental data and theoretical calculations is that if one expects to approach intrinsic relaxation times at 4.2 K and in very low magnetic fields, two things must be done: (a) a thin H_2 wall coating must be used, and (b) magnetic field gradients must be assiduously avoided. This latter requirement can be made more quantitative by use of the expressions we have written down above which apply to relaxation due to gradients in the limit $H_0 \rightarrow 0$. If we specify that the relaxation rate due to gradients must be kept below 10^{-6} sec^{-1} then the uniform component of the gradient $[\propto Y_{\ell m}(\theta, \phi)]$ must be kept below $6 \times 10^{-9} \text{ gauss cm}^{-1}$ for a 1 cm diameter sample.¹ Moreover, these same relaxation rate and sample size specifications require that any nearby ferromagnetic impurity have a magnetic moment $|\vec{\mu}| < 7 \times 10^{-10} b^{\frac{1}{2}} \text{ gauss cm}^3$ where b is the distance from the sample in cm.

Our judgment based on Cabrera's data on superconducting shields and remanent magnetization of materials⁷ is that these requirements are not impossibly severe. The use of fused quartz for the sample

container and nearby parts will probably be sufficient, although this needs to be proven.

REFERENCES

Sections A and B

1. J. M. Lockhart, F. C. Witteborn, and W. M. Fairbank, Phys. Rev. Letters 38, 1220 (1977).
2. L. I. Schiff and M. V. Barnhill, Phys. Rev. 151, 1067 (1966).
3. A. J. Dessler, F. C. Michel, H. E. Rorschach and G. T. Trammel, Phys. Rev. 168, 737 (1968).
4. F. C. Witteborn and W. M. Fairbank, Phys. Rev. Letters 19, 1049 (1967); Nature 220, 436 (1968).
5. F. C. Witteborn, Ph.D. Thesis, Stanford University (1965).
6. L. I. Schiff, Phys. Rev. B1, 4649 (1970).
7. P. P. Craig, Phys. Rev. Letters 22, 700 (1969).
8. J. M. J. Madey, Phys. Rev. Letters 22, 784 (1969).

Section C

1. L. I. Schiff, Phys. Rev. 132, 2194 (1963).
2. W. M. Fairbank and W. O. Hamilton, in *Proceedings of the Xth International Conference on Low Temperature Physics*, N. V. Zavaritsky and I. P. Krylov, eds. (Moscow, 1967), Vol IIB, p. 327.
3. See, for example, A. Abragam, *The Principles of Nuclear Magnetism*, (Oxford University Press, Oxford, 1961).
4. See, for example, *Helium Three*, J. G. Daunt, ed. (Ohio State University Press, Columbus, 1960).
5. L. D. Shearer and G. K. Walters, Phys. Rev. 139, A1398 (1965).
6. F. D. Colegrove, L. D. Shearer and G. K. Walters, Phys. Rev. 132, 2561 (1963).
7. B. Cabrera, Ph.D. Thesis, Stanford University, 1975. The shield used in our experiments was flawed. Cabrera's shields typically provide useful regions having fields of 10^{-8} - 10^{-7} gauss.
8. See J. E. Zimmerman, P. Thiene and J. T. Harding, J. Appl. Phys. 41, 1572 (1972) and R. P. Giffard, R. A. Webb and J. C. Wheatley, J. Low Temp. Phys. 6, 533 (1972) for discussions of theory and applications of rf-biased SQUID magnetometers.

9. R. Barbé, M. Leduc and F. Laloë, J. Phys. (Paris) 35, 699 (1974).
10. H. C. Torrey, Phys. Rev. 104, 563 (1956).
11. R. Barbé, F. Laloë and J. Brossel, Phys. Rev. Lett. 34, 1488 (1975).
12. W. A. Fitzsimmons, L. L. Tankersley and G. K. Walters, Phys. Rev. 179, 156 (1969).
13. I. Oppenheim and M. Eloom, Can. J. Phys. 39, 845 (1961).

APPENDIX A1

Evidence for a Temperature-Dependent Surface Shielding Effect in Cu†

J. M. Lockhart, F. C. Witteborn,* and W. M. Fairbank

Department of Physics, Stanford University, Stanford, California 94305

(Received 11 April 1977)

A large temperature-dependent transition in the magnitude of the ambient axial electric field inside a vertical copper tube has been observed. Above a temperature of 4.5 K the ambient field is 3×10^{-7} V/m or greater. Below 4.5 K, the magnitude of the ambient field drops very rapidly, reaching about -5×10^{-11} V/m at 4.2 K. We believe that these effects results from the presence of a surface electron layer on the inside wall of the tube which provides a temperature-dependent shielding effect.

A discrepancy has existed for several years between the results of the measurement by Witteborn and Fairbank (WF)¹ of the total force felt by an electron traveling along the axis of a vertical copper tube and the expected magnitude of the ambient electric field in the tube. WF measured a net force on the electron of zero to within $\pm 6 \times 10^{-12}$ V/m; this value was interpreted to be the result of the combined effects of gravity on the test electron and an ambient electric field of about -5×10^{-11} V/m. Theoretical predictions and room-temperature contact-potential results indicated that an ambient field of 10^{-6} – 10^{-7} V/m should be present. We have measured the ambient electric field present in the tube used by WF at several temperatures between 4.2 and 300 K and have found that the magnitude of the field makes a sudden transition at 4.5 K from a value consistent with that observed by WF to a value roughly four orders of magnitude larger.

At least two mechanisms act to produce an ambient electric field in a vertical metal tube. First, the fact that the tube is composed of many small crystallites results in the existence of a spatially fluctuating "patch effect" field along the axis of the tube; the rms magnitude of this field is expected to be about 10^{-6} V/m unless some ordering in the distribution of different kinds of crystallites is present. Second, the effect of gravity on the ionic lattice and the electron gas of the metal produces a uniform axial electric field in the tube.

The magnitude of the gravitationally induced field in a vertical metal tube was first calculated by Schiff and Barnhill,² who obtained the value mg/e , where m is the electron mass; this result implies that an axial field is produced by the gravitationally induced redistribution of metallic electrons but not by the differential compression of the ionic lattice caused by gravity. However, Dessler, Michel, Rorschach, and Trammell³

(DMRT) were able to show that the lattice compression should produce a much larger field Mg/e where M is the ionic mass. Later, Herring⁴ was able to reconcile the DMRT result with the approach taken by Schiff and Barnhill by taking into account certain surface effects. Other models were explored by Peshkin,⁵ Rieger,⁶ and Leung, Papini, and Rystephanick.⁷ Several room-temperature experiments were then conducted to search for stress-induced contact-potential variations in various metals; Beams,⁸ Craig,⁹ and French and Beams¹⁰ performed much of the early work. The results were in general consistent with the DMRT calculation (some of the difficulties in the interpretation of such measurements have been pointed out by Enga¹¹). By this time though, considerable supporting evidence for the validity of the WF result was available. The experiment itself yielded the proper e/m for the electron, and a related experiment measured the anomalous magnetic moment of the electron.¹² Also, the correct value of g was obtained in experiments with ions.¹³ It appeared that the low-temperature environment in which the WF experiment was conducted might have been crucial to its success. This idea led to our program of experiments in which slightly modified versions of the WF apparatus and technique were used to measure the ambient field in the copper tube at 300, 77 K, and several temperatures between 4.2 and 11 K.

Both the original apparatus and technique used by WF and the more recent modifications are described in detail elsewhere.^{14,15} The current version of the apparatus is illustrated in Fig. 1. Basically the electric field present inside a vertical electrostatic shielding tube is determined by its effect on the time of flight of a very slow electron which travels along the tube axis. A burst of low energy (<1 eV) electrons is emitted from a pulsed tunnel cathode and guided through

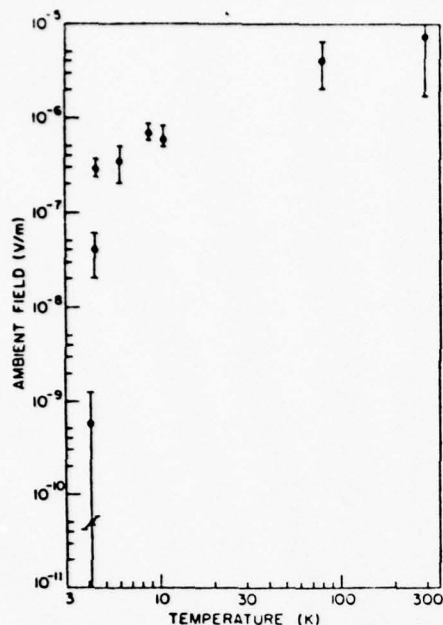


FIG. 2. The ambient electric field in the tube as a function of tube temperature. The closed circles show the present experimental results. The triangle shows the absolute value of the 1967 result of Witteborn and Fairbank, which was -5×10^{-11} V/m at 4.2 K.

means that the error curve is much closer to a rectangle function than a Gaussian.

The results in the region 4.5–11 K show an ambient field about an order of magnitude lower than that present at 77 K; the values here agree quite well with the DMRT prediction of a field of approximately 10^{-6} V/m. Below 4.5 K the very sharp transition in the ambient field can be seen. At 4.2 K we obtained a value of $(6 \pm 7) \times 10^{-10}$ V/m for the ambient field; this is consistent with the more accurate value of $-(5.6 \pm 0.6) \times 10^{-11}$ V/m obtained in the original experiment performed by Witteborn and Fairbank (WF had much more data at 4.2 K, allowing a considerably better determination of the field). The results from the range 4.2–11 K are shown as closed circles on the expanded linear temperature scale of Fig. 3.

In order to further check the 4.2–11-K results presented in Figs. 2 and 3, the time-of-flight data were analyzed by a somewhat different technique. Rather than comparing spectra taken at the same temperature but with different values of applied field in order to determine the ambient field, spectra taken at the same value of applied field but at different values of temperature were compared. This is most logically done for the

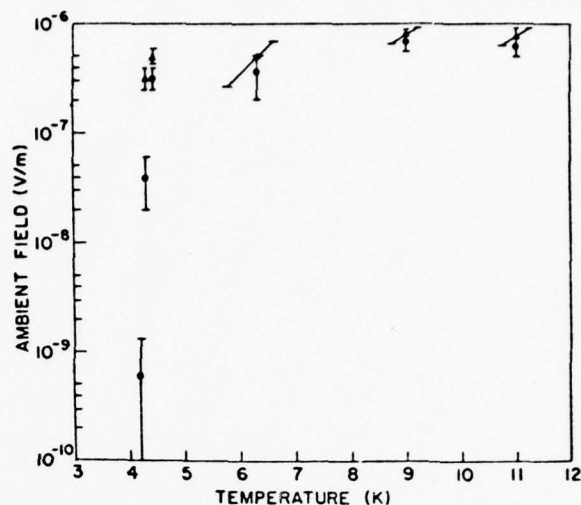


FIG. 3. An expanded view of the low-temperature results. The two sets of points are obtained using different analysis techniques, as described in the text.

case of no applied field; the results of the analysis are shown as triangles in Fig. 3. Since this latter analysis technique utilizes less of the available data than the comparison of spectra taken at a given temperature, the results are not expected to be as accurate; however, the two sets of results are in rather good agreement.

It would seem from these results that a highly temperature-dependent shielding mechanism must exist in the tube; at temperatures below 4.5 K the axis is shielded from the patch effect and lattice distortion fields while above 4.5 K the shielding is either nonexistent or only very weakly effective. There is some indication that the patch effect is either partially shielded or else is somehow reduced in magnitude below 77 K. Since the WF experiment saw a field in the tube which implied perfect shielding of the patch effect and lattice distortion fields but which agreed with the estimates for the field produced by the gravitationally induced redistribution of metallic electrons, the shielding must be accomplished by surface electrons. Condensation of residual gas on the drift tube walls is not thought to play an important role in the shielding; only 10^{-6} or so of a monolayer could be condensed since a room temperature vacuum of 10^{-10} Torr is attained before cooldown. It should be mentioned that an examination of the copper surface revealed a layer of copper oxide approximately 20 Å thick. We assume that the electrons responsible for the shielding exist on the surface of the oxide and that the

oxide serves to decouple the surface electron energy levels from the band structure of the bulk copper. It is interesting to note that the tube axis is not shielded from the field produced by passing an axial current through the walls of the tube. A search is now in progress for a theoretical model for this dramatic shielding effect.¹⁶

We gratefully acknowledge valuable discussions with Dr. John Madey and Richard Hanni concerning the nature of the surface shielding and possible mechanisms which could explain it.

†Work supported in part by the U. S. Air Force Office of Scientific Research under Contract No. F44620-75-C-0022.

*Present address: National Aeronautics and Space Administration, Ames Research Center, Moffett Field, Calif. 94035.

¹F. C. Witteborn and W. M. Fairbank, *Phys. Rev. Lett.* **19**, 1049 (1967), and *Nature (London)* **220**, 436 (1968).

²L. I. Schiff and M. V. Barnhill, *Phys. Rev.* **151**, 1067

(1966).

³A. J. Dessler, F. C. Michel, H. E. Rorschach, and G. T. Trammel, *Phys. Rev.* **168**, 737 (1968).

⁴C. Herring, *Phys. Rev.* **171**, 1361 (1968).

⁵M. Peshkin, *Ann. Phys. (N.Y.)* **46**, 1 (1968), and *Phys. Lett.* **29A**, 181 (1969).

⁶T. J. Rieger, *Phys. Rev. B* **2**, 825 (1970).

⁷M. C. Leung, G. Papini, and R. G. Rystephanick, *Can. J. Phys.* **49**, 2754 (1971); M. C. Leung, *Nuovo Cimento* **7B**, 220 (1972).

⁸J. W. Beams, *Phys. Rev. Lett.* **21**, 1093 (1968).

⁹P. P. Craig, *Phys. Rev. Lett.* **22**, 700 (1969).

¹⁰S. H. French and J. W. Beams, *Phys. Rev. B* **1**, 3300 (1970).

¹¹E. Enga, *Can. J. Phys.* **52**, 708 (1973).

¹²L. V. Knight, Ph.D. thesis, Stanford University, 1965 (unpublished).

¹³F. C. Witteborn, Ph.D. thesis, Stanford University, 1965 (unpublished).

¹⁴F. C. Witteborn and W. M. Fairbank, *Rev. Sci. Instrum.* **48**, 1 (1977).

¹⁵J. M. Lockhart, Ph.D. thesis, Stanford University, 1976 (unpublished).

¹⁶R. S. Hanni and J. M. J. Madey, private communication.

Nonlinear Optical Excitation of Surface Exciton Polaritons in ZnO

F. DeMartini

Istituto di Fisica dell'Università, 80138 Napoli, Italy, and Istituto di Fisica "G. Marconi," 00185 Roma, Italy

and

M. Colocci,* S. E. Kohn, and Y. R. Shen

Department of Physics, University of California, Berkeley, California 94720, and Materials and Molecular Research Division, Lawrence Berkeley Laboratory, Berkeley, California 94720

(Received 28 February 1977)

Dispersion and damping characteristics of surface exciton polaritons in ZnO have been measured by nonlinear optical technique. Optical mixing was used to excite surface exciton polaritons while surface roughness was used to couple the surface waves out. The results were used to deduce characteristic parameters of bulk excitons in ZnO.

The surface exciton polariton has long been a subject of extensive theoretical studies.¹ Experimental research on the subject has however been very rare. So far as we know, Lagois and Fischer² have conducted the only measurement of exciton polariton dispersion in ZnO using the method of attenuated total reflection (ATR). The difficulty lies in the fact that excitons usually exist at low temperatures and the ATR method is not easily applicable to surface polaritons with relatively short wavelengths. We have recently proposed that surface polaritons can be investigated

by nonlinear optical techniques.³⁻⁵ In this Letter, we report the first experiment on nonlinear optical excitation of surface exciton polaritons. We show that the surface exciton polariton waves are radiative because of surface roughness,⁶ and detection of the radiative surface waves enables us to measure both dispersion and damping of the surface exciton polaritons.

Surface polaritons only exist in the reststrahlen band of a crystal. For a semi-infinite anisotropic crystal *b* bounded by an isotropic medium *a*, the dispersion relation for polaritons is given⁷

APPENDIX A2

Apparatus for measuring the force of gravity on freely falling electrons[†]

F. C. Witteborn* and W. M. Fairbank

Department of Physics, Stanford University, Stanford, California 94305

(Received 30 September 1976)

An apparatus and data analysis technique for measuring the gravitational force on freely falling electrons are described. The measurement required that all forces acting on the electrons be uniform and measurable to about 10^{-11} eV/m. The electrical force along the axis of the 5-cm-diam, vertical copper tube used in the experiment was found to be about 6×10^{-11} eV/m $\pm 9\%$ when the tube was cooled to 4.2 K. Forces on electrons due to magnetic field gradients were reduced well below the electrical ones by selecting only ground state electrons for measurement. Other forces were reduced sufficiently by careful attention to the vacuum and thermal environment. The absence, at 4.2 K, of much stronger electric fields, which were expected to arise from the patch effect and from differential lattice components, contrasts strongly with measurements of electric fields near metal surfaces made at room temperature.

I. INTRODUCTION

Results of an experiment to measure the force of gravity on freely falling electrons have been reported earlier,¹⁻³ but the apparatus and the data analysis technique were not described in detail. Such a description is important at this time because of recent new results which may help to explain how such sensitive measurements are possible in apparent violation of theoretical predictions. The experimental results required that the 4.2 K metallic enclosure surrounding the evacuated free fall region was free of electric fields larger than about 10^{-11} V/m except for a uniform field that cancelled the force of gravity on electrons to within 9%. The cancellation is consistent with the theoretical prediction for the electric field set up by gravitational compression of electrons in the walls of the metal enclosure,⁴ but not with the fields expected from the patch effect^{5,6} on metal surfaces or from strain-induced fields produced by differential lattice compression^{6,7} which were predicted to be 10^5 times larger than the field set up by the electrons in the walls. Other experimental techniques have been used at room temperature and with significantly greater lattice compression⁸⁻¹¹ to measure the strain-induced electric fields near metals. The magnitude of the measured values was generally in agreement with lattice compression theories. One conclusion that was tentatively reached from these experiments was that the lattice compression field might be shielded at low temperature either by adsorption of gases to the walls, or by an electronic surface state, or by a combination of these effects.^{3,12-14} Further evidence that the shielding effect is real is provided by new low temperature free-fall data¹⁵ obtained using essentially the original apparatus but with improved methodology. Since the new results confirm the ability of this technique to measure forces on freely falling charged particles as small as 10^{-11} eV over a linear distance of nearly 1 m, this paper was

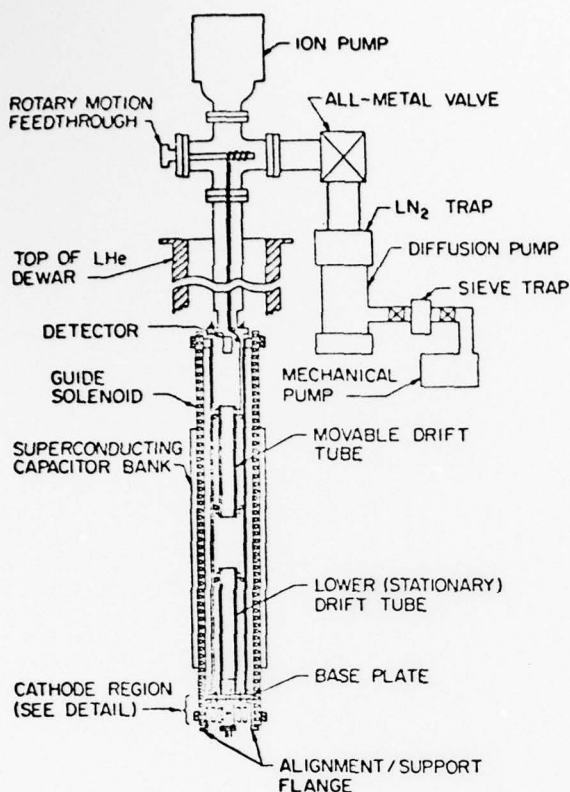
written to make important details of the technique generally available.

A brief summary of the experiment is given here as a guide to the remainder of the paper, where the rationale for essential features of the apparatus is discussed. Electrons are emitted in a short burst from a cold cathode located at the bottom of a long, vertical copper tube in a vacuum chamber with 4 K walls (Fig. 1). The electrons are constrained to move vertically through the tube by an axial magnetic field. A windowless, 14-dynode electron multiplier detector at the top produces a measurable voltage pulse at its anode each time an electron hits its entrance. This pulse is amplified and stored in a multichannel analyzer (MCA) in a memory channel appropriate to the time of flight (TOF) of the electron through the drift tube. The experiment is repeated many times until a distribution of flight times has been stored in the memory of the MCA. Known forces can be applied to the electrons by running currents axially through the drift tube; these forces alter the TOF distributions. A study of time-of-flight distributions for several such known forces enables one to determine what intrinsic vertical forces are present in the tube.

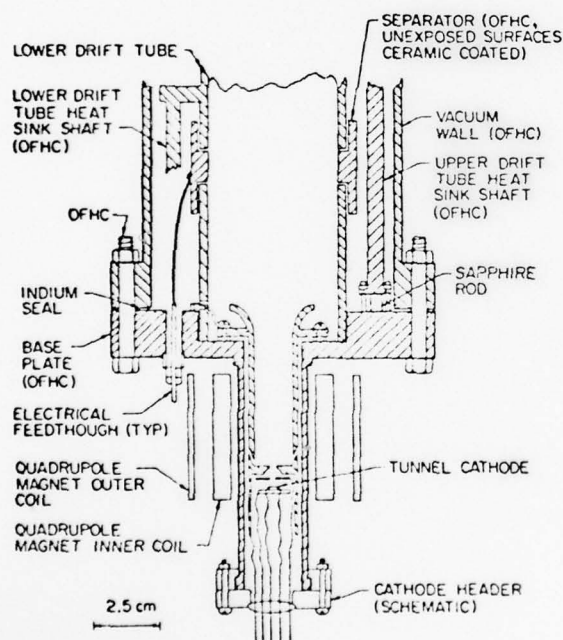
In addition to the time-of-flight mode of operation (discussed further in Sec. V), the apparatus was designed to operate in another mode to provide an alternative method for making the desired measurements. This mode is described in Sec. VI. The reduction of forces and the cathode characteristics affect both modes of operation and, therefore, are described first in Secs. II-IV.

II. REDUCTION OF ELECTRIC STRAY FIELDS

In order to measure forces comparable to that of gravity on freely falling electrons it was necessary to produce an enclosure free of electric fields greater than



(a)



(b)

FIG. 1. (a) Schematic diagram of free fall apparatus. Each drift tube is 90 cm long. The liquid helium level was usually above the detector during measurements. (b) Details of the cathode region. OFHC denotes parts made of oxygen-free high-conductivity copper.

10^{-11} V/m. The enclosure had to be metal (conducting) to prevent buildup of static charge. Since the field induced by even one electron within a few meters of a conductor exceeds the desired value, it was necessary to choose a geometry in which forces were balanced

by symmetry or else to work with a prohibitively large apparatus. An electron moving along the axis of a perfectly uniform, infinitely long cylinder in zero gravity is in a field-free region, because the induced surface charge is symmetric around the free electron. The electron can be constrained to stay near the axis by a uniform axially directed magnetic field. In a cylinder of finite length with end caps at potentials slightly different from the cylinder, the axial electric field resulting from the end caps drops off approximately as $\exp(-2.4z/a)$, where z is the distance from the nearer end and a is the radius. Thus an attenuation of 10^{10} is achieved in 9.6 radii. By orienting the tube vertically, the gravitational force would be the only axial force felt, provided that magnetic field gradients and electrical fields due to irregularities in materials were negligible.

A polycrystalline metal will exhibit variations in the electric potential just outside the surface, because the surface is made up of many crystal faces (patches) which have different work functions. If the patches were arranged in a regular array the variations in potential as one moved parallel to the surface would drop exponentially with distance from the surface. There is no reason to expect such a regularity in patch distribution, so that potential variations due to random excesses of one type of patch over another must be expected. A simple analysis^{3,5} predicts that along the axis of a tube of radius a potential variations of

$$\Delta\Phi = (3A\tau^2/8\epsilon_0^2a^2)^{1/2}$$

should exist, where A is the patch area and τ/τ_0 is the potential change across the dipole double layer which is associated with the patch. τ/ϵ_0 varies typically by about 0.1 V from one crystal surface to another. Patch sizes of a few hundredths of a millimeter are expected for normally processed metals. These parameters result in excessively large variations in $\Delta\Phi$ for reasonable values of drift tube radius (a few centimeters). For example if a is 2.5 cm, τ/ϵ_0 is 0.1 V, and A is 10^{-6} cm², then $\Delta\Phi$ is 2.5×10^{-5} V, which is much too large. Reducing the patch area to atomic dimensions brings A down to 10^{-16} cm², so $\Delta\Phi$ becomes about 10^{-10} V. An amorphous surface masks the underlying crystal structure and may have a value of A approaching atomic dimensions.

In order to produce a long cylinder (hereafter called the drift tube) with an amorphous interior surface and very uniform interior dimensions, OFHC copper was electroformed onto a carefully machined, polished aluminum mandrel. The mandrel was 6061 aluminum, 91 cm long, and 5 cm diameter with variations less than 0.0003 cm. Prior to bulk deposition of copper the aluminum was flash plated in a copper phosphate solution. After deposition was complete, the exterior surface of the drift tube was machined to provide a uniform wall thickness of 0.40 cm along the length of the tube. Then the mandrel was dissolved and the tube was rinsed. Three drift tubes were made. Even the best of these has observable variations in surface texture, but

the crystal surfaces are smaller than 10^{-4} cm. Even prior to the construction of the drift tubes, it was recognized that the patch effect appeared to represent a fundamental barrier to the experiment, so a small, pilot-model time-of-flight apparatus was built and tested.⁵ It was found that the fields present at the center of a 2-cm-diam drift tube cooled to 4.2 K were less than 10^{-10} V/m. The theoretical explanation for this fortuitous behavior is still under study but may be related to the same effect which shields the lattice compression field.

Another possible source of undesired electric field is the Thompson emf. The potential variation ΔV_T due to a temperature difference ΔT along a homogeneous metal surface is given by $\Delta V_T = \sigma_T \Delta T$, where σ_T is the Thompson coefficient. This is typically a few microvolts per degree for metals. Thus ΔT must be less than 10^{-5} K for the desired measurements. If the drift tube were in direct contact with the liquid helium cooling bath a temperature gradient of up to 0.34 K/m would exist because of variation in liquid helium boiling point with pressure.¹⁶ Thus it is necessary that the drift tube be in good contact with the bath at only one location and be well insulated from its vacuum enclosure everywhere else. To accomplish this, a 0.6-cm-thick copper flange was shrink fitted to the ends of each drift tube (where a slight dimensional change would not degrade the electrostatic uniformity of the interior). 0.6-cm-diam OFHC copper rods extend from these flanges to sapphire wafers mounted on the 1.9-cm-thick, OFHC copper flange at the bottom of the vacuum enclosure. Indium was held under compression between each of the copper-to-sapphire joints. Heat leaks into the copper drift tube or heat generated by running electric current through the drift tube (and associated wires) had to be smaller than the amount given by $\Delta Q/\Delta t = KA dT/dx$, where K is the thermal conductivity of annealed OFHC (about 10 W/cm/K at 4.2 K)¹⁷, A is the cross-sectional area of the drift tube (6.84 cm^2), and dT/dx is 10^{-7} K/cm. Thus we require that $\Delta Q/\Delta t$ be less than 6.84×10^{-6} W. This is easily satisfied when no current is run through the drift tube; however, when an axial electric field is applied, power is dissipated, particularly at the junctions of the wires to the drift tubes. Since the drift tube resistance at 4.2 K was $4.5 \times 10^{-7} \Omega$ (in 1966), a current, I , of 2×10^{-4} A produced an axial field of 10^{-10} V/m. The power dissipated at the junctions (of resistance R_j) at the ends of the tube is $I^2 R_j$. If we require that the thermally generated electric field be less than one-tenth of the electrically generated field in this case, then R_j must be less than 171Ω , a condition that is easily satisfied. The same requirement for the 4.5×10^{-7} V/m field produced when I is 1 A is that R_j be less than 0.31Ω . Contacts were made with copper straps wrapped under tension around the ends of the drift tubes. The current-carrying wires were lead-covered copper of approximately 0.1 cm diameter. The superconducting vacuum feedthroughs also used lead-covered copper conductors as shown in Fig. 2, so that the total resistance was much below 0.1Ω . Thus all

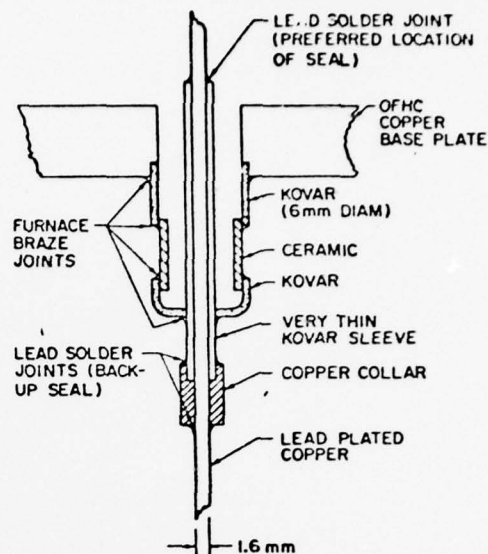


FIG. 2. Superconducting high vacuum feedthrough.

heat loads to the drift tube were small enough to avoid interference with the required measurements.

Two electrostatic effects arise from the fact that the copper tube is oriented vertically in a gravitational field. First, the electrons in the metal walls redistribute themselves to set up an electric field that cancels the gravitational force on a free electron in the tube.⁴ In addition, a much larger field is expected because of the redistribution of the positive ions needed to support their overlying weight.^{6,7} The shielding of the field at low temperature has been demonstrated experimentally^{5,15} but is not well understood. The apparatus is well suited to further studies of this effect.

A calculation of the thermal fluctuations in the electric field¹⁸ experienced by the electrons travelling along the axis of a 4.2 K drift tube appeared to show that electric fields smaller than 10^{-7} V/m could not be measured by the time of flight method described in this paper. This calculation was found to be erroneous. In an erratum¹⁹ the limiting electric field was redetermined to be on the order of 10^{-14} V/m, which no longer affects the free fall experiments.

III. REDUCTION OF MAGNETIC FIELD GRADIENTS AND OTHER FORCES

Spatial or temporal variations, ΔB , in the coaxial magnetic field required to constrain the electrons to the center of the drift tubes result in potential variations given by

$$\Delta\Phi = 2\mu_B \Delta B(n + 0.5 + (sg/2)s),$$

where $\mu_B = 0.56 \times 10^{-8}$ eV/G is the Bohr magneton, $g_s \approx 2.0023$ is the gyromagnetic ratio, $s = \pm 0.5$ is the spin quantum number, and n is a positive integer. The $n + 0.5$ arises from the solutions to the Schrödinger equation for orbital motion in the plane perpendicular

to the magnetic field. The values of n depend on the collisional history of the electrons as they are injected into the bottom of the drift tube. The distribution of n values is discussed in the section on the cathode. It suffices here to say that most will be greater than or equal to one. In any case we require

$$\Delta B < 10^{-3} \text{ G} / [n + 1/2 \pm g_s/4]$$

to keep $\Delta\Phi \leq 10^{-11}$ eV. The requirements placed on magnetic shielding needed to exclude external fields, on materials and electrical circuits used within the shielding enclosure, and on the uniformity of the coaxial solenoid were considered too severe to ensure that ΔB would be less than 10^{-3} G. This restriction may be relaxed to allow ΔB as large as 1 G for electrons having $n = 0$ and $s = -1/2$, the ground state. A large field gradient near the cathode was employed to assure that slow electrons were in the ground state. If the electrons start out in a high magnetic field, B' , and at the same electrostatic potential as that of the drift tube, all those not in the ground state will accelerate as they leave the high field and pass through the drift tube with kinetic energy equal to $2\mu_B(B' - B)[n + 1/2 + sg_s/2]$, where B is the magnetic field in the drift tube. The ground state electrons actually decelerate slightly as they enter the low field region since their kinetic energy changes by $2\mu_B(B' - B)[1/2 - g_s/4]$ a negative quantity. In the free fall apparatus B' was 3000 G. It was maintained by a superconducting quadrupole magnet consisting of two concentric cylindrical windings. The outer winding was allowed to go superconducting in the field B maintained by the 3-m-long superconducting solenoid used to constrain electrons to the center of the drift tubes (Fig. 1). The inner winding (i.d. = 3.2 cm, o.d. = 4.7 cm) was then turned on and allowed to go superconducting at the current level calculated to produce B' in the presence of the opposing field produced by the outer cylinder of the quadrupole. This arrangement ensured that the magnetic potential change in 72% of the lower 1 m drift tube was below 0.5 G (3×10^{-12} eV potential variation for ground state electrons).

A much better reduction of magnetic fields at long distances from the cathode could have been achieved by allowing the outer winding of the cathode to go superconducting at some intermediate value of the inner field. This was not realized until recently. Allowing the outer winding to go superconducting before turning on the inner winding results in an unnecessary magnetic trap extending into the lower drift tube for non-ground state electrons. Subsequent decay of their magnetic states (by radiation or collision) can result in escape of these electrons from the traps. This may be an important source of that component of TOF distributions that did not appear to respond to applied forces. Methods for handling trapped electrons in the data analysis are discussed in Appendix A.

Another unwanted force associated with the use of magnetic fields to constrain the paths of electrons

results from imperfect alignment of the axis of the solenoid with that of the drift tube. Mechanical tolerances and uncompensated external fields will produce a finite angle between the axes which will result in the electrons moving away from the center of the drift tube. An electron of charge e displaced by a small amount y from the center of a conducting cylinder of radius a will experience a radial image attraction force given by $eE = e^2 y / 4\pi\epsilon_0 a^3$. Charges in crossed electric and magnetic fields drift with velocity given by $\mathbf{v} = \mathbf{E} \times \mathbf{B} / B^2$. The additional motion leads to an orbital magnetic moment given by $\mu = ev_0 y / 2 = e^2 y^2 / 8\pi\epsilon_0 B_z a^3$. When B is 20 G, a is 2.54 cm, and y is 5×10^{-2} cm, then μ is 0.88×10^{-27} A m² or 0.55×10^{-12} eV/G. This is well below the anomalous magnetic moment so that the resulting interaction with field gradients will not be important. Since B and z are not precisely aligned, a fraction, y/z , of the "radial" electrostatic field is actually z directed. We require the field given by $E_z = ey^2 / 4\pi\epsilon_0 a^3 z$ to be less than 10^{-11} V/m. This holds if y is less than 3.4×10^{-4} m. Since machining tolerances 10 times smaller are readily achieved, the required alignment was provided by mechanically supporting the magnet frame with alignment collars attached to the drift tube housing.

An orbital magnetic moment results if the electron does not enter the drift tube exactly on its axis. As in the preceding discussion, this stems from the lateral force of attraction to its image in the wall of the drift tube, and the same expression is valid for the magnetic moment. If we plan to allow B -field variations as large as 0.1 G, then r , the distance from the axis, must be held to 0.7 cm to hold potential variations to 10^{-11} eV. Note, however, that the magnetic field strength drops by a factor of about 100 from the electron emitter to the drift tube region. Since $B_z \pi r^2$ is a constant, the radius of the emitter must be below 0.07 cm if r is to stay below 0.7 cm in the drift tube.

Yet another force to be considered is that of collisions with gas in the drift tube. The particle concentration of background gases in the drift tube had to be made low enough to make unlikely any collisions that would change the energy of electrons by more than 10^{-11} eV. One reason for doing the experiment at 4.2 K was to reduce outgassing from the walls, thus greatly reducing the background gas pressure. In addition the cold walls served as a pump by condensing all gases except helium and hydrogen. The only gas likely to be present was helium. Hydrogen, whose equilibrium vapor pressure is about 10^{-6} Torr at this temperature,²⁰ is pumped very efficiently by the ion pump used in the experiment and was probably present in much smaller quantities than helium gas.

The interaction of greatest importance in determining the vacuum requirement is the attraction of the electron to the induced dipole moment of the helium atom. The dielectric strength K of helium gas is about 1.000065.²¹ The polarizability α is $(K-1)\epsilon_0/n_0$, where n_0 is Loschmidt's number, 2.69×10^{23} , so for a helium

atom, is about $0.21 \times 10^{-40} \text{ F m}^2$. The electric field strength due to the electron is $E = q/4\pi\epsilon_0 r^2$, where r is the distance from the electron. Thus the induced dipole moment is given by $p = \alpha E = \alpha q/4\pi\epsilon_0 r^2$. The potential of the dipole is $p \cos\theta/4\pi\epsilon_0 R^2$, where R is the distance from the atom and θ is the angle between the observation point and a line connecting the atom and the electron. For the electron, of course, θ is 0 and R is r . The potential energy of an electron near a helium atom is thus $-\alpha q^2/(4\pi\epsilon_0)^2 r^4$. This quantity exceeds 10^{-11} eV when $r < 0.72 \times 10^{-5} \text{ cm}$. The cross section σ for undesirable collisions is therefore $1.66 \times 10^{-10} \text{ cm}^2$. We want the mean free path $1/n\sigma$ to be greater than h which is 90 cm, the drift tube length. This determines the background pressure. Evidently we must have $n < 1/\sigma h = 6.7 \times 10^7 \text{ cm}^{-3}$, which corresponds to a pressure of $2.9 \times 10^{-11} \text{ Torr}$ at 4.2 K.

During most of the experiments the pressure was monitored by a gauge in the warm part of the system. If no condensable gases were involved we would read a pressure in the gauge P_g related to that in the drift tube P_d by $P_g = (300/4.2)^{1/2} P_d$; thus the desired P_g in this case is $2.4 \times 10^{-10} \text{ Torr}$.

The vacuum enclosure is constructed of inorganic, bakeable materials throughout to ensure that insulating deposits would not form on drift tube surfaces. All gaskets are indium or copper. The enclosure surrounding the drift tubes is copper with ceramic-to-metal and glass-to-metal feedthroughs at the end flanges. No ferromagnetic materials were used in the drift tube region. No superconducting loops were allowed except the guide solenoid and cathode field solenoids. Magnetic materials could not be tolerated because of the need to keep B -field variations below 0.1 G in the drift tube region. The entire region below the detector is immersed in liquid helium. The vacuum plumbing above the detector is 300-series stainless steel. An 80 liter/sec ion pump is at the top (Fig. 1). The all metal bakeable valve is closed except during the initial "rough" pumping period. The rough pumping system is not oil free, but is used for only 2 h, during which the liquid nitrogen cold trap is kept full. During this rough pumping period the apparatus is kept at room temperature or hotter. A 100 C bakeout was used when the system was first assembled. The rough pumping is continued to a pressure of about 10^{-7} Torr . Then the ion pump is turned on. Once it has degassed itself the all-metal valve is closed. After two weeks the pressure drops to the neighborhood of 10^{-9} Torr . Cooling of the drift tube region reduces the pressure to values too small to measure confidently with commercial gauges but certainly below 10^{-11} Torr in the warm portion.

The 3-m-long, 15-cm-diam guide solenoid is made of superconducting niobium-zirconium wire wound on a titanium core. It is specified to be uniform to 10^{-4} of its average field throughout the drift tube region. Use of a persistent current, superconducting magnet helps to achieve a time-constant B field and minimizes power

dissipation in the liquid helium bath. This saves liquid helium and minimizes thermal gradients.

The entire assembly is supported by a cable wound on a hand driven winch which is used to lower it into a Dewar.

The liquid helium Dewar itself is 5 m deep, 30 cm in diameter. It is made of aluminum except for its fiber-glass neck tube. A liquid nitrogen-cooled radiation shield surrounds the helium reservoir. Surrounding the Dewar is a 43-cm-diam magnetic shield made of an inner layer of Netic and an outer layer of CoNetic. The outer layer shields the inside from external fields. The inner layer prevents the relatively high fields used in the experiment from saturating the CoNetic. The shields are reasonably round and uniform ($\pm 0.2 \text{ cm}$) and extend well beyond the drift tube so that they do not degrade the uniformity of the guide solenoid. The shields are periodically degaussed.

IV. CATHODE

The requirements on the cathode are (1) that there be an observable number of ground-state electrons as low in energy as 10^{-11} eV , (2) that the electrons be emitted in pulses of width equal to 10^{-3} sec or less and at no other time, (3) that not much heat be introduced into the system, and (4) that very little gas be emitted in operating the cathode. The tunnel diode emitters²² satisfy these criteria. Those provided to us by J. W. Hall of General Electric Laboratories and similar devices built in our own lab consist of a layer of aluminum oxidized to a depth of roughly 75 \AA , covered in turn by an evaporated gold layer about 100 \AA thick. A positive voltage (2–6 V) applied to the gold layer causes electrons from the aluminum to tunnel into the unoccupied conduction band of the oxide layer. Currents of 3 mA and pulse widths of 1 msec are easily maintained without degrading the cathode. Most of the electrons are stopped in the gold layer, but a small fraction (typically 10^{-4} for sustained pulsed operation) passes through the gold into the vacuum. A space charge removal aperture, 1 mm diameter and typically operated at +30 V, was placed about 2 mm above the tunnel diode. A grounded aperture was placed just above the first aperture to reduce field penetration into the drift tube region. The kinetic energy distribution of the electrons and the fraction in the ground state have been shown³ to satisfy requirement (1) for the cathode. This argument is outlined below.

Under the conditions discussed above, the cathode emits about 2×10^9 electrons per pulse. Their energies are distributed with a roughly thermal distribution characteristic of 3000 K because of collisions suffered in the gold and aluminum oxide layers of the cathode.²³ The corresponding energy distribution half-width is on the order of 0.3 eV. The voltage between drift tube and cathode emitting surface is set so that electrons near the peak of the distribution pass with almost zero

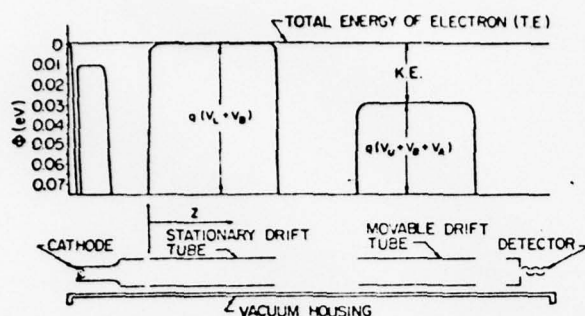


FIG. 3. Potentials seen by electron as it passes through the free fall apparatus (shown schematically along the abscissa). In the TOF mode V_0 is adjusted so that the kinetic energy (KE) is large in the movable drift tube.

kinetic energy over the potential hill presented by the drift tube. Since only TOFs longer than 10^{-3} sec are recorded, an energy range less than 10^{-5} eV is sampled from the distribution. In this range the number ΔN passing over the potential maximum in the drift tube with energy ΔW or less is

$$\Delta N = CN_0 \Delta W, \quad (1)$$

where C is a constant depending on the characteristic temperature and how close to the emission peak the voltage between drift tube and cathode can be set, and N_0 is the total number of electrons emitted. To obtain a rough estimate of $\Delta N/N_0$ we note that $\Delta N/N_0$ is about 1 when ΔW is 0.3 eV, so $\Delta N/N_0$ is $\Delta W/0.3$ eV. Thus to get one electron with energy of 10^{-11} eV or less requires that N_0 exceed 3×10^{10} electrons. The fraction in the ground state is approximately $\mu_B B/kT \approx 10^{-4}$ when B is 3000 G and T is 3000 K. Thus, 3×10^{14} electrons would be required, or about 10^5 pulses. If the pulses are emitted at 1-sec intervals (to permit the full TOF distribution to be obtained) it would take 30 h of data collection to get a reasonable probability of collecting one electron with 10^{-11} or less under the assumptions made above. However, the emitted electrons are not frozen in temperature after leaving the cathode. Because of the Coulomb force, they continue to interact as they enter the drift tube. The high velocity electrons leave quickly, so the interaction is taking place between relatively low energy electrons. The characteristic temperature may be much lower than that of the emitted distribution and continues to decrease with time after the initial emission from the cathode until only two or fewer electrons remain. Consequently the number of low energy electrons is enhanced considerably. Evidence for this enhancement is provided by the TOF distributions discussed in the next section.

V. TIME-OF-FLIGHT METHOD

The directly measured quantity in this experiment is the distribution of electron flight times. Such distributions may be measured for various uniform applied electric fields, E_A , produced by running currents axially along the drift tube. The expected effect on the TOF

distribution is obtained in general from the energy integral

$$t = \left(\frac{m}{2} \right)^{1/2} \int_0^h \frac{dz}{[W - qV(z)]^{1/2}} \quad (2)$$

and Eq. (1). $V(z)$ is the potential in the drift tube; W , the electron total energy, is always greater than $qV(z)$, over the length h of the drift tube. Outside the drift tube $W - qV(z)$ is so large that the contribution to t may be ignored. If we assume that $V(z) = zE_A$ and neglect other contributions such as fringe fields, then Eq. (2) yields

$$W(t) = \frac{q^2 E_A^2 t^2}{8m} + \frac{m}{2} \frac{h^2}{t^2} + \frac{qhE_A}{2}. \quad (3)$$

The time differential, given by

$$\Delta W(t) = \left(\frac{q^2 E_A^2 t}{4m} - \frac{mh^2}{t^3} \right) \Delta t, \quad (4)$$

may be used in Eq. (1) to give

$$\frac{\Delta N}{\Delta t} = CN_0 \left(\frac{q^2 E_A^2 t}{4m} - \frac{mh^2}{t^3} \right). \quad (5)$$

These expressions are valid only for $t < (2mh/qE_A)^{1/2}$, since larger values would imply negative values of $W - qV(z)$ which prevent the electron from reaching the detector. The t^{-3} term is dominant throughout the distribution except at the cutoff time $t = (2mh/qE_A)^{1/2}$, so it is clear that C is negative. While the t^{-3} behavior was observed in some distributions, a slower dropoff (i.e., $t^{-\alpha}$ with $\alpha < 3$) was more typical. Computer fits to the distribution that account for the fringe fields in the drift tube, the applied force, the possibility of electron detention in potential traps, and a constant background of noise, are discussed in Appendix A. They gave values of α from 1.6 to 2.1 for the distributions actually used in determining the effective force in the drift tube. The remaining discussion of the TOF method is concerned with the electrical circuitry and procedures used in data collection.

The TOF method requires only one drift tube and is therefore not sensitive to small, timewise variations in potential relative to the remaining portions of the apparatus where the electrons are moving fast (see potential diagram, Fig. 3). A direct current source is required to produce the axial electric fields from 10^{-11} V/m to 10^{-6} V/m which are applied to the moving electrons. The drift tube resistance at 4.2 K was found originally to be $4.5 \times 10^{-7} \Omega$ using a four-wire hookup which eliminated most of the problems of lead resistance and thermal emf. (Several years of thermal cycling have raised this value by a factor of 2.) The currents required thus ranged from 10^{-4} to 2 A with 10% accuracy required at the lowest range. Since it was not known *a priori* that the intrinsic electric field in the drift tube would be small, it had to be assumed that the smallest force on the electron might occur when a large current was applied (to cancel the intrinsic

field). This required that the current supply be stable to 10^{-5} A even when providing 2 A. A Fluke model 382A was used for this purpose. As noted in the section on reduction of electric fields, it was important to minimize the heat generated in the lead-in wires, so superconducting wires (lead-covered copper) were used within the vacuum enclosure. The lead-in wire going to the top of the drift tube was straight, parallel to the drift tube axis and as far from it as possible (about 4 cm) to minimize the transverse magnetic field that would be felt by drifting electrons when current was being carried. At a 4 cm separation a current of 2 A in the wire produces a transverse magnetic field of 10^{-1} G, which adds vectorially to the axial field of 20 G to move the electrons 0.4 cm away from the axis after 80 cm of travel. From the discussion in Sec. III the allowable limit is 0.033 cm, so currents higher than 0.15 A can be used only if the total resultant applied force on the electron exceeds 100 mg (6×10^{-9} V/m). The remaining circuitry for the time-of-flight mode is conventional and shown schematically in Fig. 4. A ramp voltage triggers successively the following electronic functions: (1) quenching of the detector by shorting the first two dynodes to ground to prevent overloading by the initial burst of electrons, (2) emission of the electrons from the cathode, (3) reactivating the detector, and (4) initiation of the multichannel scaling in 100 or 400 successive channels (counting for a preset time of 20–2000 μ sec in each channel). When the multichannel analyzer (MCA) finishes scaling in its last channel, it puts out a pulse which is used to initiate another ramp so that the cycle is repeated. This is continued for some preset time or until data collection is terminated manually. In recent experiments,¹⁵ a timer circuit was used in conjunction with the MCA and the drift tube current supply to collect data successively under four different values of electric field in the drift tube. The TOF distribution for each electric field was stored in 100 channels of the 400 available. This was done to average out effects of slowly varying conditions (e.g., liquid helium level, building noise) in the experiment. The electric field was changed every 10 min but data were collected for several hours, so that TOF distributions for each applied force were obtained under roughly similar conditions. It was found to be helpful to turn off the ion pump during data collection to avoid occasional noise counts from ultraviolet light emitted from the pump. This had no observable effect on the pressure when the system was helium cooled.

VI. MOVABLE DRIFT TUBE METHOD

Two criticisms of the TOF method of measuring mg on electrons (or positrons) are (1) its requirement that the electric fields due to patches and other surface irregularities be shielded by an empirically verified but theoretically unexplained mechanism, and (2) the inability to repeat the experiment with the

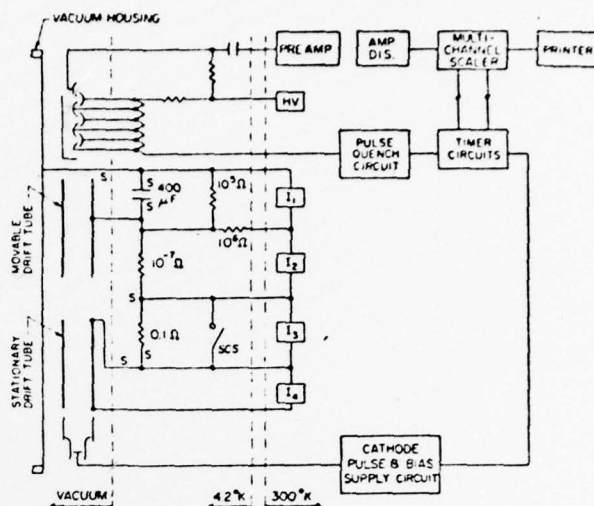


FIG. 4. Block diagram of electrical system.

apparatus inverted to ensure that nongravitationally induced fields were not inherent in the system. These deficiencies can be corrected, at the expense of introducing a large electrostatic trap in the path of the electrons, by placing a movable drift tube between the stationary (lower) drift tube and the detector, as shown in Fig. 1. The difference between the kinetic energy of a particle of charge q , mass M in the upper tube, and that in the lower tube is given by

$$\Delta KE = q(V_L - V_U) - qV_A + mgxq/e - Mgx, \quad (6)$$

where e is the electron charge, m the electron mass, V_A is the applied voltage across the resistor which electrically couples the tubes, and V_U and V_L are the intrinsic potential maxima of the upper and lower tubes, respectively (Fig. 3). V_U and V_L depend on contact potentials, tube dimensions, and strain-induced potentials, but not on the spatial separation, x , of the potential maxima in the two tubes. Note in particular that the strain potential does not change with the position of the upper tube to the extent that g is constant over the dimensions of the experiment. The term $-mgxq/e$ is the Schiff-Barnhill potential,⁴ which must arise if the tubes are electrically connected. Note that for an electron, we expect $-mgxq/e + Mgx = 0$, but for a positron with normal gravitational properties $-mgxq/e + Mgx = 2mgx$.

The principle of this method is that V_A can be adjusted until $\Delta KE = 0$ and that when $\Delta KE = 0$ the number of slow electrons reaching the detector is maximized regardless of the shapes of the potential hills in the upper and lower tubes. The slow electron count is greater when the electrons are forced to move slowly in two parts of the apparatus rather than one as can be seen by increasing h in Eq. (5).

The movement of the upper tube must be accomplished without introducing additional unknown potentials. These could arise from changing the position or angle of the axis of the tube, resulting in forces

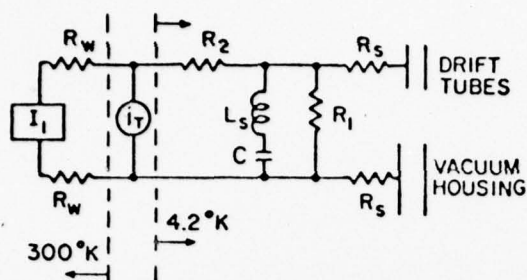


Fig. 5. Circuit diagram of drift tube bias and filter.

caused by finite values of y discussed in Sec. III. To prevent excursions in y of more than about 0.2 mm, the tube was constrained laterally by ball bearings held firmly against the walls of the copper vacuum enclosure by copper races attached directly to each end of the drift tube. The upper tube was suspended from a ceramic coupling by a long stainless steel cable attached to a drum in the warm part of the system. The drum was coupled to an external crank through a commercial bellows-wobble stick rotary motion feedthrough. Temperature changes could also introduce changes in potential. The ball bearings were made of ceramic for thermal and electrical insulation. A flexible copper strap arrangement provided thermal contact to the helium bath at the base flange of the lower drift tube regardless of the position of the upper tube. The flexible copper had a cross section equivalent to a 0.6-cm-diam copper rod, a length of 3 m, and was thermally coupled to the base flange through sapphire to provide electrical insulation. The flexible portion of the copper had to be kept taut at all times to prevent electrical contact with the vacuum enclosure. This was done with a pulley and spring arrangement. Resistance thermometers were installed at each end of the upper tube to determine whether the upper drift tube was indeed in good contact with the helium bath. The wires to these resistors had to be insulated from everything else with small glass beads and run over a separate set of pulleys. This arrangement eventually broke and has since been removed. However, while it was still intact they showed that the upper drift tube was in excellent contact with the helium bath. Finally it was necessary to ensure that spatial variations of the magnetic field were as small over the entire travel of the upper tube (1 m) as those discussed in Sec. 3.

The electrical circuit for the movable drift tube mode is shown in Fig. 4. The potential difference between upper and lower tubes is adjusted by changing the current I_2 through R_2 , the $0.88 \times 10^{-7} \Omega$ resistor connecting the tubes. The resistance could not be larger than $10^{-7} \Omega$ without introducing excessive Johnson noise ($>10^{-11}$ V) at the highest frequencies (10^6 Hz) that might affect the experiment. The rather high frequency stems from the possibility that the potentials in the two tubes are peaked so that electron travel time across the peaks would be very fast ($\sim 10^{-4}$ sec). Since it must be possible to "remove" the upper tube electrically for the

TOF mode by applying at least 0.01 V (positive for electrons), a 0.1Ω resistor is also in the circuit. It may be shorted out by a superconducting switch. The switch consists of a 0.1Ω resistor in parallel with a long length of lead-plated rhenium wire. The length is noninductively wound and placed inside a small solenoid. When magnetic fields above the critical field for lead are applied by running current in the solenoid, the switch is "open" to a value much larger than 0.1Ω . Closing the switch is accomplished by turning off the solenoid current. This allows the circuit to be used in the movable drift mode, since there is no Johnson noise across the superconductor.

The most severe electrical problem for the movable drift tube method stems from noise in the circuit that maintains the bias of approximately 0.01 V or higher between the drift tubes and the vacuum housing. Electrons see the housing as they traverse the gap between the drift tubes. If the drift tube bias voltage changes during the time of the traverse ($\sim 10^{-5}$ sec) the electron energy will change accordingly, nullifying the ability to match the drift tube potentials. The potentials are to be matched to 10^{-11} V and frequencies on the order of 10^5 Hz are of greatest concern. Noise at lower frequency will have proportionately smaller effect on the electrons because they will go from one tube to the other while the noise voltage has ranged through only a fraction of its full amplitude. Noise at frequencies well above the reciprocal of the transversal time will tend to average out as the electron moves from the region enclosed by the vacuum tube to that enclosed by the drift tube. Thus we must have a 10^{-2} V dc supply with less than 10^{-11} V rms noise in the 10^5 – 10^7 Hz range.

Consider the circuit in Fig. 5. The voltage is to be developed by sending current I through resistance R_1 . I is limited by the need to not dissipate too much power in the helium bath that cools R_1 . The capacitor C shunts the high frequency Johnson noise in R_1 . The Johnson noise voltage across a complex impedance²⁴ is

$$\langle V^2 \rangle = \int_0^\infty 4kT \operatorname{Re}(f) df, \quad (7)$$

where $\operatorname{Re}(f)$ is the real part of the complex impedance. For the parallel RC circuit we have

$$\operatorname{Re}(f) = R/(1 + R^2 C^2 4\pi^2 f^2).$$

Integrating Eq. (7) gives

$$\langle V^2 \rangle = \frac{2kT}{\pi C} (\tan^{-1} 2\pi f_2 R_1 C - \tan^{-1} 2\pi f_1 R_1 C).$$

For large values of $2\pi f_1 RC$ this simplifies to (8)

$$\langle V^2 \rangle = \frac{kT}{\pi^2 R_1 C^2} \left(\frac{1}{f_2} - \frac{1}{f_1} \right).$$

Before choosing values for R_1 and C , other limitations imposed by external circuitry must be examined. The current I will have low impedance noise from the supply (on the order of 10^{-7} A) plus thermoelectrically gen-

erated noise and pickup of electromagnetic radiation in the wires and junctions between the 4.2 K network and the room temperature electronics. The RC circuit serves as a filter for the noise from these sources which we shall assume to be 10^{-7} A at $f_1 = 10^5$ Hz. If these variations in current are sinusoidal, the resulting rms voltage fluctuations are

$$V = \frac{1}{2} \frac{RI}{(1 + R^2 4\pi^2 f^2 C^2)^{1/2}} \approx \frac{I}{4\pi f C}, \quad 2\pi f RC \gg 1. \quad (9)$$

This suggests that a very large capacitor is desirable. So far the Johnson noise across the resistances of the wires R_s has not been considered. R_s must be smaller than $10^{-7} \Omega$ to avoid exceeding 10^{-11} V Johnson noise. Consequently all interconnecting wires from the filter to the drift tubes and housing were made of (superconducting) lead-plated copper. The drift tubes and housing themselves had sufficiently low resistance (below $10^{-6} \Omega$). The connections from the wires to the drift tube and the housing were made by superconducting clamps (split to avoid forming a closed current loop around the drift tubes). The plates of the capacitor itself had to be superconducting for the same reason that the interconnecting wires did. This placed a volume constraint on the capacitor since it had to fit inside the Dewar. The largest practical size using a bank of rolled capacitors (lead-tin and Mylar sheet) was about 400 μ F. The resulting rms noise voltage at $f = 10^5$ Hz in Eq. (9) is 2×10^{-10} V. This was reduced by a large factor for noise from high impedance sources by the series resistor R_2 . The introduction of R_2 (necessarily inside the helium bath) placed a constraint on how fast the voltage across R_1 could be changed. The time constant CR_2 must not exceed a few minutes if the bias level is ever to stabilize during the experiment. Thus R_2 must be on the order of $10^6 \Omega$ or lower.

The requirement that $\langle V^2 \rangle \leq 10^{-22}$ V² in Eq. (8) at $f_1 = 10^5$ Hz is consistent with $C = 400 \mu$ F at 4.2 K if $R_1 > 3 \Omega$. A value of $R_1 = 10^3 \Omega$ was found to be consistent with all the above criteria and with low power dissipation.

The inductances associated with the superconducting wires in Fig. 5 have not yet been included in the calculation of Johnson noise. The Johnson noise in a purely reactive circuit element is zero so the inductance of the superconducting leads from R_1 to the drift tubes and vacuum housing does not contribute noise. However the inductance in the capacitor leads is part of the filter and is the dominant reactive element at frequencies above 10^4 Hz if we assume a lead inductance of about 1.5 μ H for a 1-m-long, 1-mm-diam wire. If we include the inductance in the capacitor leads, the complex impedance is given by

$$Z = \frac{R_1[2\pi fL - (2\pi fC)^{-1}]^2}{R_1^2 + [2\pi fL - (2\pi fC)^{-1}]^2} + \frac{\sqrt{-1} R_1^2[2\pi fL - (2\pi fC)^{-1}]}{R_1^2 + [2\pi fL - (2\pi fC)^{-1}]^2}.$$

If we neglect $1/2\pi fC$ relative to $2\pi fL$ and make the approximation $2\pi fL/R_1 \times f \ll 1$, then the Johnson noise is

$$\langle V^2 \rangle = \frac{16\pi^2}{3} \frac{kTL^2}{R_1} (f_2^3 - f_1^3). \quad (10)$$

If the upper frequency of concern is 10^6 Hz, R_1 is $10^3 \Omega$, L is 1.5 μ H, and $T = 4.2$ K, then $\langle V^2 \rangle^{1/2}$ is 2.6×10^{-10} V. Reactive elements of the noninductively wound wire resistor R_1 were considered to be of lesser importance. It is clear from Eq. (10) that a great advantage can be gained by reducing L . A factor of 10 reduction might be achieved by redesign of the existing capacitor bank and its connection to R_1 .

The inductive leads to the superconducting capacitor also seriously impair the filtering capability of the network in Fig. 5. A noise current source of 10^{-7} A at 10^6 Hz would produce about 6×10^{-7} V noise. On the other hand, when the noise is from a high impedance source, the resulting noise voltage is divided by $2\pi fL/R_2$, so that noise in the room temperature electronics up to 10^{-5} V can be tolerated. It is clear that further efforts to use the free fall apparatus in the movable drift tube mode will require careful attention to this problem. The results from the original effort to operate in this mode² were promising but required much longer integration times than expected because of noise. This appears to have resulted from noise current sources introduced by the power supply used for the relative drift tube biasing (I_2 in Fig. 4). Reduction of common mode noise by use of additional filtering in the room temperature portion of the electronics appears to be a feasible solution to the problem.

VII. FURTHER APPLICATIONS OF THE APPARATUS

Recent experiments by Lockhart¹⁵ using the TOF method with the free fall apparatus and improved methodology have verified the shielding of the patch field and the strain-induced field at 4.2 K. A modification which permits temperature control of the lower drift tube enabled him to demonstrate that the shielding disappears at higher temperatures.²⁵ A source of slow positrons is being developed. It is expected to perform free fall experiments on positrons with appropriate modifications to the original electron free fall apparatus.

APPENDIX: FIVE PARAMETER FUNCTIONS FOR COMPUTER NONLINEAR LEAST-SQUARES FIT TO TOF DATA

In this appendix an electron TOF distribution function is derived for a source containing a mixture of cooling electrons (interacting as they expand against the Coulomb force of receding electrons) and trapped electrons. The distribution law [Eq. (5)] in Sec. V may be integrated from t to infinity to give an equation of the form

$$N(t) = A(t^{-1} - bt)^{2c} + f(t_{\max} - t), \quad (11)$$

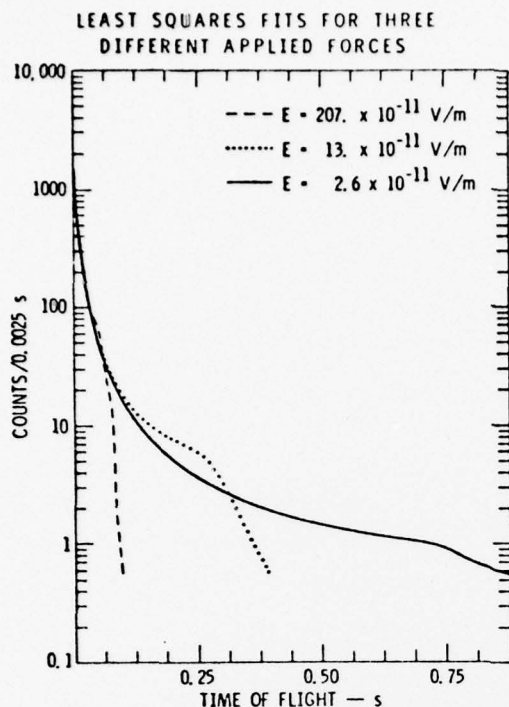


FIG. 6. $N'(t)$ vs TOF for three different applied forces.

where b is $qE/2mh$, and A is 0 if t exceeds $b^{-1/2}$. $N(t)$ represents the total number of electrons arriving after time t until t_{\max} (t_{\max} is chosen to be several times $b^{-1/2}$). f represents constant background noise. It would have appeared as a constant in Eq. (5) had noise been considered. A is determined from the total number of electrons in the distribution. We now generalize b to include all constant, uniform forces in the drift tube by making it a free parameter. We also allow c to be a free parameter to account for the cooling of the electrons as the initial pulse expands in the drift tube.

So far, $N(t)$ does not include the effect of trapped electrons escaping after $t = 0$. We will account for them now by assuming that all electrons are trapped (at least for a very short time) and escape at time τ with probability $P(\tau)$. Then the TOF distribution function becomes

$$N(t) = \int_0^t A(t, \tau) [(t - \tau)^{-1} - b(t - \tau)]^{2c} \times P(\tau) d\tau + f(t_{\max} - t), \quad (12)$$

where A is a constant for $t - \tau < b^{-1/2}$, and $A = 0$ for $t - \tau \geq b^{-1/2}$.

Two forms for $P(\tau)$ are common for the escape of particles from traps. One is an exponential function; it is appropriate when the probability of release is directly proportional to the number of particles remaining in the trap. Another, appropriate to escape resulting from collisions between particles in the trap, is a power law whose exponent depends on the number of particles involved in the collision. The latter was chosen here and the exponent d was allowed to be a free parameter. Thus we have $P(\tau) = \tau^{-d}$.

An additional modification to the distribution function is required to properly account for the fact that the electric field outside the drift tube penetrates inside as discussed in Sec. II. This requires inserting a better approximation to $V(z)$ in Eq. (2). The most significant contribution to the TOF will come where the electron moves most slowly. If there is some constant force $f = qE$, then the maximum potential comes at one end of the drift tube where we approximate the junction of the exponentially decaying penetrating potential $e^{-2.42/a}$ and the linear potential aEz by the quadratic $k_1(z - z_m)^2$, where z_m is the point where the electron is moving most slowly. The time spent by the electron while moving over this region is

$$\delta = \left(\frac{m}{2} \right)^{1/2} \int_0^{z_1} \frac{dz}{[W - k(z - z_m)]^{1/2}}, \quad (13)$$

where z_1 is the location where the linear potential begins. Thus the effective length of the drift tube is reduced to $h - z_1$. The constants k and z_m are determined from known potentials and the geometry of the experiment. δ may be treated as a small correction to the TOF, $t - \tau$, so that the energy integral for the conditions used in the experiment is

$$t - \tau = \delta + \int_{z_1}^h \frac{dz}{[W + qE(z - z_m - 0.208a)]^{1/2}},$$

and may be inverted (approximately) to give

$$W = -0.208 a q E$$

$$+ \frac{m}{2} \left[\frac{h - z_1}{(t - \tau - \delta)} - \frac{qE}{2m} (t - \tau - \delta) \right]^2. \quad (14)$$

The right side of Eq. (14) may be substituted for the term $[(t - \tau)^{-1} - b(t - \tau)]^2$ in Eq. (12). Integration must be done iteratively since δ is a function of W [see Eq. (13)]. The distribution function may be compared to the data by using a nonlinear least-squares-fit computer program to adjust the values of A , b , c , d , and f to give an optimum fit by the chi-square test. Initial estimates for the parameters must be provided to use such a program.

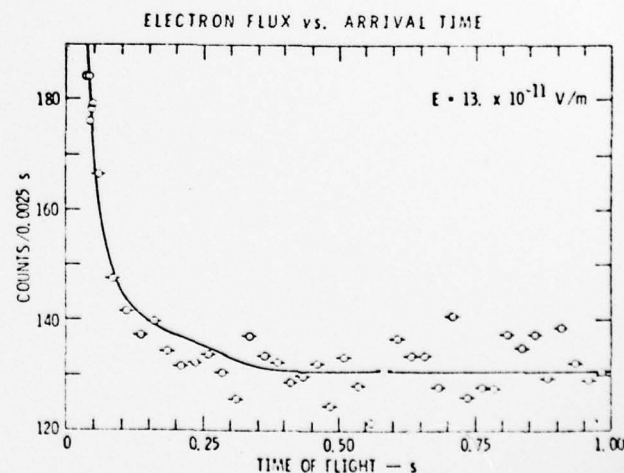


FIG. 7. $N'(t)$ vs TOF compared with data.

This was done by using the differential distribution function $N'(t) = N(t + \Delta t) - N(t)/\Delta t$ at small values of t to determine d and c and at the largest values to determine f . The parameter A is determined from d , c , f , and the empirical value of $N(t)$ for some small values of t . The parameter b could have been estimated by using the applied force, but to avoid prejudicing the answer it was initialized at zero. The answer obtained by this procedure is not necessarily unique because chi-square has more than one minimum for a nonlinear, multiparameter function. However, by initializing b at zero and using the first deep minimum in the chi-square test, the same physical significance could be attached to the determination of b from each data set. Plots of the function $N'(t)$ for several values of b and typical values of A , c , d , and f are shown in Fig. 6. A computer fit of $N'(t)$ to actual TOF data is shown in Fig. 7. This is one of numerous fits used to establish that the force of gravity on electrons in a vacuum is the same as that inside a metal.

ACKNOWLEDGMENT

It is a pleasure to thank Dr. James Lockhart for useful discussions and a careful review of the manuscript.

* Present address: NASA, Ames Research Center, Moffett Field, CA 94035.

¹ F. C. Witteborn and W. M. Fairbank, Phys. Rev. Lett. 19, 1949 (1967).

[†] Supported in part by the U.S. Air Force Office of Scientific Research.

- ² F. C. Witteborn and W. M. Fairbank, Nature 220, 436 (1968).
- ³ W. M. Fairbank, F. C. Witteborn, J. M. J. Madey, and J. M. Lockhart, in *Experimental Gravitation*, edited by B. Bertotti (Academic, New York, 1974), p. 310.
- ⁴ L. I. Schiff and M. V. Barnhill, Phys. Rev. 151, 1067 (1966).
- ⁵ F. C. Witteborn, thesis, Stanford University, 1955 (unpublished).
- ⁶ A. J. Dessler, F. C. Michel, H. E. Rorschach, and G. T. Trammell, Phys. Rev. 168, 737 (1968).
- ⁷ C. Herring, Phys. Rev. 171, 1361 (1968).
- ⁸ J. W. Beams, Phys. Rev. Lett. 21, 1093 (1968).
- ⁹ P. Craig, Phys. Rev. Lett. 22, 700 (1969).
- ¹⁰ S. H. French and J. W. Beams, Phys. Rev. B 1, 3300 (1970).
- ¹¹ E. W. Guptill, Can. Phys. 49, 3150 (1971).
- ¹² G. T. Trammell and H. E. Rorschach, Phys. Rev. B 2, 4761 (1970).
- ¹³ W. A. Harrison, Phys. Rev. 130, 1606 (1969).
- ¹⁴ M. Peshkin, Phys. Lett. A 29, 181 (1969).
- ¹⁵ J. M. Lockhart, F. C. Witteborn, and W. M. Fairbank, in *Proceedings of the 14th International Conference on Low Temperature Physics*, 4, edited by M. Krusius and M. Vuorio (Elsevier, New York, 1975), p. 274.
- ¹⁶ R. T. Swim, in *Advances in Cryogenic Engineering*, 5, edited by K. D. Timmerhaus (Plenum, New York, 1960), p. 498.
- ¹⁷ R. L. Powell and D. O. Coffin, in *Advances in Cryogenic Engineering*, 1, edited by K. D. Timmerhaus (Plenum, New York, 1960), p. 262.
- ¹⁸ H. J. Maris, Phys. Rev. Lett. 33, 1177 (1974).
- ¹⁹ H. J. Maris, Phys. Rev. Lett. 33, 1594 (1974).
- ²⁰ R. E. Honig and H. O. Hook, RCA Rev. XXI, 360 (1960).
- ²¹ *Handbook of Chemistry and Physics*, 45th Ed., edited by R. C. Weast (Chemical Rubber Co., Cleveland, 1964), p. E-33.
- ²² J. W. Hall, II, *Research, Development and Fabrication of Tunnel Cathodes, Final Report* (General Electric Receiving Tube Dept., Owensboro, KY, 1964).
- ²³ R. E. Collins and L. W. Davies, *Solid State Electronics*, 7 (Pergamon, London, 1964), pp. 445-453.
- ²⁴ F. N. H. Robinson, *Noise in Electronic Circuits* (Oxford U. P., London, 1962), p. 31.
- ²⁵ J. M. Lockhart, thesis, Stanford University, 1976 (unpublished).

APPENDIX A3

Experimental Evidence for a Temperature-Dependent
Surface Shielding Effect Inside a Copper Tube

by

James Marcus Lockhart

(enclosed under separate cover)

APPENDIX B

PHOTON COUNTER PERFORMANCE ESTIMATES

The performance of the photon counter, specifically, the noise temperature, quantum efficiency, and response time are determined by the cavity temperature and the relative rates at which the electrons and the cavity walls absorb from the radiation field.

In calculating the quantum efficiency the cavity walls can be assumed at 0 K. The rate of absorption of radiation by the cavity walls is then

$$\frac{dE}{dt} \text{ cavity losses} = - \frac{\omega}{Q_c} E$$

where E is the stored energy in the cavity and Q_c the unloaded cavity Q . Similarly, electrons moving through the cavity will extract energy in transitions from the $n=0$ to $n=1$ cyclotron level at a rate

$$\frac{dE}{dt} \text{ cyclotron transitions} = - \frac{\omega}{Q_E} E$$

where Q_E can be defined in terms of the transition probability per electron and the average number of electrons in the cavity. Finally, the Q of the coupling hole can be defined in terms of the rate of loss of energy through the hole:

$$\frac{dE}{dt} \text{ coupling hole} = - \frac{\omega}{Q_H} E$$

The quantum efficiency is then the ratio of the rate of absorption of radiation by the electrons to the total rate of absorption by the electrons and cavity walls:

$$\begin{aligned}\text{Quantum Efficiency} &= \frac{-(E\omega) \frac{1}{Q_E}}{-(E\omega) \frac{1}{Q_E} + \frac{1}{Q_C}} \\ &= \frac{Q_C}{Q_E + Q_C}\end{aligned}$$

The quantum efficiency approaches unity for $Q_C \gg Q_E$. For the photon counter under construction, $Q_E \ll Q_C$ so that the quantum efficiency is approximately equal to (Q_C/Q_E) .

The noise temperature T_N can be defined as the source temperature required to double the detector output measured at zero source temperature. For the photon counter this translates to the source temperature required to double the energy of the radiation field in the cavity.

For a cavity and source at radiometric temperatures T_C and T_S , respectively, and for an electron distribution all of whose members are in the ground state. The rate of transfer of energy to the radiation field is:

$$\frac{dE}{dt} = -\frac{\omega E}{Q_E} - \frac{\omega}{Q_H} (E - KT_S) - \frac{\omega}{Q_C} (E - KT_C)$$

At equilibrium $(dE/dt) = 0$ and the equilibrium energy is:

$$E = \frac{KT_S}{2} + \frac{Q_H}{2Q_C} KT_C$$

where we have assumed ideal matching, e.g.,

$$\frac{1}{Q_H} = \frac{1}{Q_C} + \frac{1}{Q_E}$$

The radiometric noise temperature, T_N , is then given by

$$T_N = \frac{T_C}{1 + (Q_C/Q_E)}$$

The counting rate can be expressed in terms of the equilibrium energy in the radiation field (E) and the electronic Q:

$$\begin{aligned}\text{Counting Rate} &= \frac{E}{h\omega} \frac{\omega}{Q_E} \\ &= \frac{1}{Q_E} \frac{K}{h} \frac{T_S}{2} + \frac{Q_H}{2Q_C}\end{aligned}$$

The response time can be defined as the time required for E to approach equilibrium after a sudden change in T_S . The response time is evidently:

$$\begin{aligned}\text{Response Time} &= \frac{1}{\omega} \frac{1}{Q_H} + \frac{1}{Q_E} + \frac{1}{Q_C}^{-1} \\ &= \frac{Q_H}{2\omega} \text{ assuming an ideal match.}\end{aligned}$$

The cavity in the detector under construction is resonant in the TE_{011} mode. The cavity is in the form of a cylinder with a 5 mm diameter and an adjustable top plate. The height is 5 mm for operation at $\lambda = 3.8$ mm and 0.5 mm for operation at $\lambda = 1$ mm. The calculated Q_C for copper is 10^4 at 3.8 mm and 2×10^3 at 1 mm for room temperature operation. Although the Q will be limited by the anomalous skin effect a significant improvement can be anticipated at cryogenic temperatures.

The rate of absorption of energy by the electrons can be calculated from first order perturbation theory. The result for the electronic Q is:

$$Q_E = \frac{2\pi v f^2}{528 n_e} \frac{1}{2Q_L^2} + 2 \frac{\Delta H}{H}^2 + \frac{1}{\pi f t}^2 \quad 1/2$$

where $v \equiv$ cavity volume in m^3

$f \equiv$ operating frequency in Hz

$n_e \equiv$ mean number of electrons in the cavity

$Q_L \equiv$ loaded cavity Q $\frac{1}{Q_L} = \frac{2}{Q_C} + \frac{1}{Q_E}$ assuming matched conditions

$\frac{\Delta H}{H} \equiv$ magnetic field homogeneity within the cavity

$t \equiv$ transit time of the electrons through the cavity

Factors determining Q_E include Q_C , the number of trapped electrons and the magnetic field homogeneity. Assuming the room temperature cavity Q, 10^4 electrons/cm and a homogeneity $(\Delta H/H) 10^{-4}$ the electronic Q ranges from 3×10^5 at 3.8 mm to 1.3×10^7 at 1 mm.

Quantum efficiency, noise temperature and response time improve with decreasing Q_E . Calculated values for these quantities as a function of wavelength are tabulated in Table 2 in the text. In view of the improvement in cavity Q anticipated at 4 K these values should be regarded as lower bounds for the quantum efficiency and upper bounds for the noise temperature and response time.